REGENERATION

The pioneer transcription factor Zelda controls the exit from regeneration and restoration of patterning in *Drosophila*

Anish Bose, Keaton Schuster†, Chandril Kodali, Surabhi Sonam, Rachel K. Smith-Bolton*

Copyright © 2025 The Authors, some rights reserved; exclusive licensee American Association for the Advancement of Science. No claim to original U.S. Government Works. Distributed under a Creative Commons Attribution NonCommercial License 4.0 (CC BY-NC).

Many animals can regenerate tissues after injury. While the initiation of regeneration has been studied extensively, how the damage response ends and normal gene expression returns is unclear. We found that in *Drosophila* wing imaginal discs, the pioneer transcription factor Zelda controls the exit from regeneration and return to normal gene expression. Optogenetic inactivation of Zelda during regeneration disrupted patterning, induced cell fate errors, and caused morphological defects yet had no effect on normal wing development. Using Cleavage Under Targets & Release Using Nuclease, we identified targets of Zelda important for the end of regeneration, including genes that control wing margin and vein specification, compartment identity, and cell adhesion. We also found that GAGA factor and Fork head similarly coordinate patterning after regeneration and that chromatin regions bound by Zelda increase in accessibility during regeneration. Thus, Zelda orchestrates the transition from regeneration to normal gene expression, highlighting a fundamental difference between developmental and regeneration patterning in the wing disc.

INTRODUCTION

The phenomenon of regeneration after damage or loss of a limb, organ, or tissue involves regrowth of the tissue, followed by cell fate respecification and differentiation to restore the original structure and function. Some animals such as axolotls have incredible regenerative capacity and can restore lost limbs and transected spinal cords (*1*). However, in most mammals, while some tissues and organs such as the liver, digit tip, and skeletal muscles can regenerate, their regenerative potential reduces with age (*2*), and tissues such as limbs, joints, and the heart regenerate very poorly (*3*–*5*). Thus, understanding the damage-response mechanisms in organs and appendages that are capable of regeneration can lead to a broader understanding of how regeneration occurs in different contexts and how it may be applied to induce wound healing and repair. While numerous studies have focused on how regeneration begins and progresses in a variety of model organisms, little is understood about how regeneration ends and normal cell fate and function are restored.

The *Drosophila* wing imaginal disc, the larval precursor of the adult wing, has the intrinsic ability to regenerate (*6*). During wing disc regeneration, the damaged tissue proliferates because of the activity of multiple damage-response and proregeneration signals, including reactive oxygen species, c-Jun N-terminal kinase (JNK) and p38 signaling, Janus kinase/signal transducers and activators of transcription signaling, and WNT signaling (*6*, *7*). Upon tissue damage, many cell fate markers are lost and remain absent during regenerative growth (*7*). The damage response ends, regeneration signaling abates without stimulating overgrowth, and correct patterning and cell fate gene expression are restored before the animal enters metamorphosis (*8*). However, the regulatory mechanisms that control the end of regeneration and establishment of cell fate remain poorly understood, raising the question: How does the regenerating tissue exit regeneration and return to normal development?

Here, we show that the pioneer transcription factor *zelda* (*zld*) controls repatterning after regeneration in the wing imaginal disc. Zld is essential during embryogenesis for the maternal-to-zygotic transition, pattern formation, sex determination, and cellularization (*9*–*15*). In the embryo, Zld binds loci that require its activity for accessibility and loci that remain accessible even in the absence of Zld (*13*). The loci that remain accessible are enriched for binding sites for a second pioneer transcription factor, GAGA factor/*Trithorax-like* (GAF/*Trl*), suggesting that they may act in either a coordinated or redundant manner (*13*). Subsequent work suggested that these loci transition from being bound by Zld to being bound by GAF and that they are not required for each other's ability to localize appropriately (*16*). Outside of the embryo, zygotic *zld* is important for maintaining type II neuroblasts in an undifferentiated state in the fly brain (*17*). Thus, Zld plays an important role during key developmental transitions or changes in cell behavior. In this study, we show that Zld is dispensable for normal wing development. However, we hypothesized that Zld might play a role in the transition from the damage response to normal development at the end of disc regeneration.

Notably, we found that Zld is important for controlling tissue patterning and cell fate specification at the end of regeneration through regulating specific cell fate determinants and ensuring a timely transition from regeneration gene expression to developmental gene expression. We found that reducing or impairing Zld disrupted margin and vein cell fate, induced posterior-to-anterior (P-to-A) fate transitions, and interfered with integrin expression, resulting in adult wings with blisters. In addition, our Cleavage Under Targets and Release Using Nuclease (CUT&RUN) analysis of regenerating wing discs suggests that other pioneer factors such as Forkhead Box A (FoxA)/Fork head (Fkh) (*18*) and GAF/Trl (*19*) may bind many of the same loci. Reduction of Fkh and GAF during regeneration produced phenotypes similar to loss of Zld, and GAF and Zld were

Cell and Developmental Biology, University of Illinois at Urbana-Champaign, Urbana, IL 61801, USA.
*Corresponding author. Email: rsbolton@illinois.edu
†Present address: Department of Molecular Pathobiology, New York University School of Dentistry, New York, NY 10010, USA.

detected in proximity to each other. Analysis of existing assay for transposase-accessible chromatin with sequencing (ATAC-seq) data suggests that Zld-bound regions increase in accessibility over the course of regeneration. Thus, Zld is crucial for reestablishing and stabilizing cell fate, regulating patterning, and ensuring correct wing architecture, allowing a regenerated wing disc to undergo metamorphosis to generate the adult wing blade.

RESULTS

A spatiotemporal system to cause tissue damage in the wing imaginal disc

To explore how cell fate and pattern are reintroduced in late regeneration and identify the mechanisms that control gene expression during this phase of repair, we used a spatiotemporal damage system to induce damage and regeneration in the *Drosophila* wing imaginal disc (*8*, *20*). This method uses a GAL4 transgene inserted in the *rotund* (*rn*) locus (*21*), which is expressed in the pouch of wing discs, the primordium of the adult wing blade (Fig. 1A). GAL4 activity is suppressed at 18°C by a temperature-sensitive Gal80 ($Gal80^{ts}$) (*22*). A temperature shift to 30°C in the early third instar (day 7 after egg lay) allows the GAL4 to express the proapoptotic *UAS-reaper* (*rpr*) (*23*) to induce cell death. After 24 hours, shifting the temperature back to 18°C allows $Gal80^{ts}$ inhibition of *rpr* expression (Fig. 1A). The regenerating wing pouch, marked by expression of *nubbin* (*nub*), had very few cells remaining at 0 hours of recovery time (R0). The wing pouch steadily increased in size from 24 hours (R24, early regeneration) through 48 hours (R48, mid-regeneration) and was almost back to its normal size by 72 hours (R72, late regeneration) (Fig. 1A).

Several such methods of inducing damage have been used to identify changes in patterning and cell fate that occur in the regenerating wing disc (*7*, *8*, *24*). The regenerating pouch loses expression of markers for various cell fates, which are not reestablished until the end of regeneration (*7*, *8*). For example, the margins of the adult wing (Fig. 1B) are established by expression of the gene *cut* (*ct*) at the dorsoventral (D/V) boundary of the wing disc downstream of Notch signaling (Fig. 1C) (*25*, *26*). After ablation, Ct expression was absent at R24 (Fig. 1D), although the D/V boundary and Notch signaling were present (*8*). Ct expression partially returned at R48 (Fig. 1E) and was completely restored by R72 (Fig. 1F).

In addition, the regenerating tissue loses intervein and provein marker expression (*7*, *8*, *24*). The intervein regions between the veins in the adult wing can be identified in the developing disc by expression of *blistered* (*bs*) (*27*, *28*), which was absent in the pouch at R24, was mostly absent in the pouch at R48 except for a few Bs-positive cells at the edges of the pouch, and was lastly restored at R72 in five of eight wing discs (Fig. 1, G to K). Vein and intervein gene expression is regulated by Notch signaling activity (*29*), which we detected using the *E*(*spl*)*Mb-CD2* Notch signaling reporter (*30*), and is expressed at the D/V boundary and in the intervein regions during normal development (Fig. 1, L and M). At R24, the Notch activity reporter was expressed in a thick stripe around the D/V boundary, which persisted at R48 (Fig. 1, N and O). By R72, expression was restored to the D/V boundary and intervein regions in three of five discs (Fig. 1P), which is similar to previous reports (*8*). We assessed the provein cell identity (Fig. 1Q) using expression of the Notch signaling ligand *Delta* (*Dl*) (Fig. 1R) (*7*, *31*). At R24, Dl was expressed in a thin stripe at the presumptive D/V boundary (Fig. 1S), which becomes broader and more diffuse by R48 (Fig. 1T). Normal Dl expression returned by R72 in 4 of 10 discs (Fig. 1U), while the remaining discs had incomplete Dl expression that was missing sections such as the L2 and L5 proveins.

The WNT family ligand *wingless* (*wg*) is essential for wing blade, margin, and hinge formation (Fig. 1V) (*32*–*34*) and is expressed along the D/V boundary and in an inner ring (IR) and an outer ring (OR) around the wing pouch (Fig. 1, V and W) (*35*). At R24, Wg was expressed throughout the regenerating blastema, as previously reported (Fig. 1X) (*8*). The Wg expression pattern began transitioning into the D/V boundary and hinge rings at R48 (Fig. 1Y), often passing through intermediate expression patterns not observed during normal development (*8*) and by R72 returned to its normal pattern (Fig. 1Z). Thus, cell fate genes progress through nondevelopmental expression patterns during regeneration before returning to their correct expression patterns. As noted, not all regenerating discs had completely normal cell fate gene expression by R72, which was reflected in the resulting adult wings that had minor errors in patterning (*36*–*38*).

Zld regulates cell fate and patterning during regeneration

We wondered what factors facilitate the restoration of normal developmental gene expression by 3 days after damage. Pioneer transcription factors are capable of such a large-scale reprogramming and developmental transition (*39*). For example, the pioneer factor SRY-related HMG-box 4 (SOX4) is expressed after damage in the liver and can induce cellular reprogramming during damage-induced metaplasia (*40*). In addition, the pioneer factor SOX9 reprograms embryonic epidermal stem cells into hair follicle stem cells and, in a basal cell carcinoma model, reprograms adult epidermal stem cells into hair follicle stem cells, repeating this developmental transition (*41*). Furthermore, the pioneer factor *early growth response* (*egr*) is important for regeneration in acoel worms, and the pioneer factors Sox2 and Krüppel-like factor 4 (Klf4) are important for regeneration in retinal ganglion cells (*42*). Thus, we hypothesized that the exit from regeneration could be orchestrated by a transcription factor that can exert pioneering function to open regions near developmental genes to restore patterning gene expression. One such candidate was Zld, one of the most well-characterized *Drosophila* pioneer factors, which controls the embryonic maternal-to-zygotic transition (*9*).

Previous work suggested that the *zld* transcript is not uniformly expressed in wing discs (*14*). However, our immunostaining in a late third instar undamaged disc shortly before pupariation showed that Zld protein is expressed uniformly throughout the developing disc, which was confirmed by imaging a disc with endogenously tagged green fluorescent protein (GFP)::Zld (Fig. 2A and fig. S1A) (*43*). Zld expression levels remained unchanged throughout the mid-late third instar stage in wing discs (fig. S1B). Zld expression was slightly but not statistically significantly elevated in the regenerating pouch at R24 (Fig. 2B). By contrast, Zld expression was markedly increased at R48 within the regenerating region and remained upregulated at R72 (Fig. 2, C to E). We also observed a similar upregulation in *zld* mRNA as assessed by quantitative polymerase chain reaction (qPCR) (Fig. 2F).

To determine Zld's role during regeneration, we used a previously reported fly line in which the endogenous Zld is tagged with cryptochrome 2 (CRY2) at its N terminus (CRY2::Zld) to optogenetically inactivate Zld (*11*). We inactivated Zld by shining blue light-emitting diode (LED) light on the larvae during R0 to R72 (fig. S1C). Exposing undamaged w^{1118} larvae that did not contain

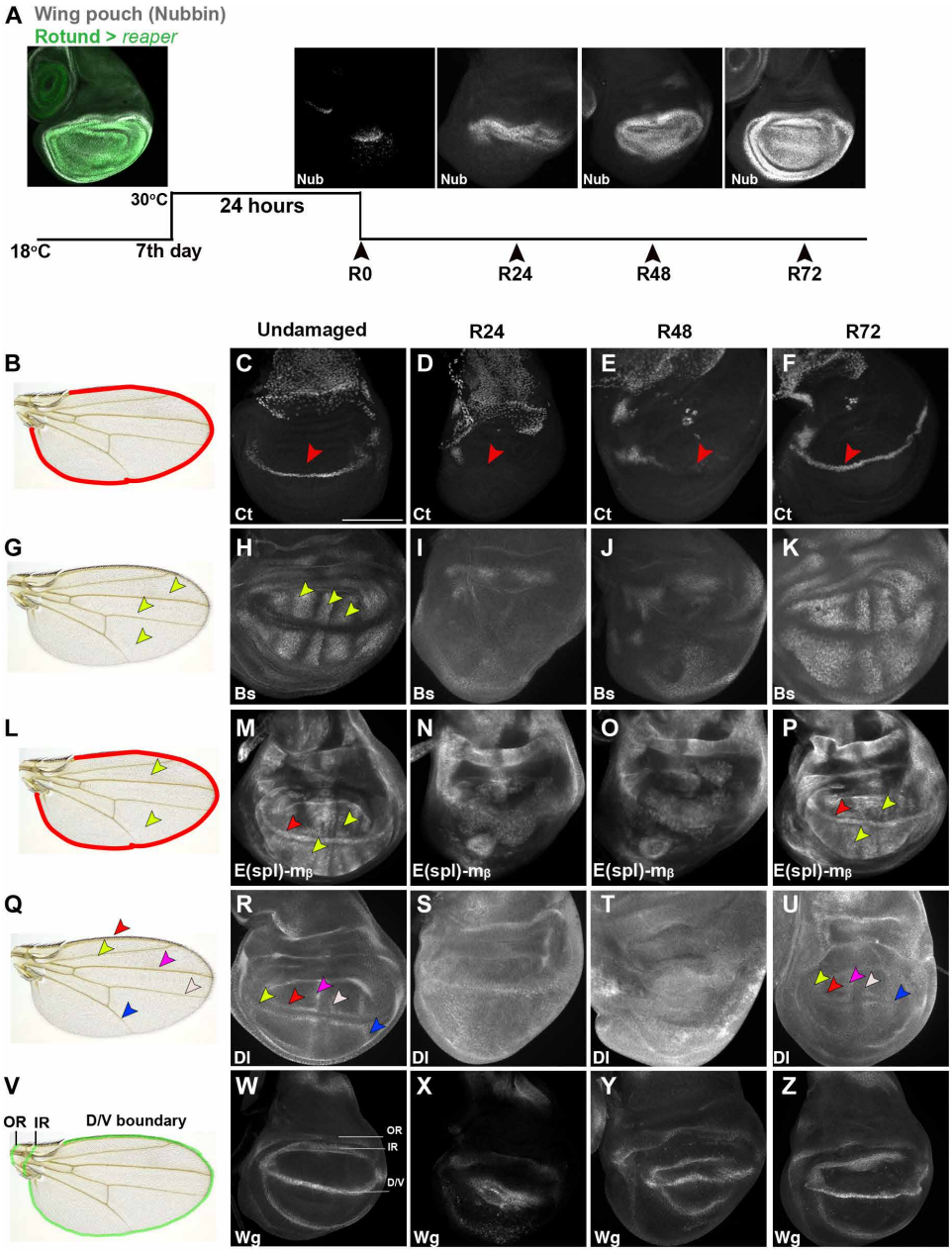

Fig. 1. Gene expression during regeneration. (**A**) Wing pouch of third instar wing discs with immunostaining for Nubbin (Nub) (gray) and *rn* > green fluorescent protein (GFP) (green) demarcating where *rpr* was expressed. (**B**) Adult wing with margin outlined in red. (**C** to **F**) Ct expression at the D/V boundary (red arrowheads) in undamaged (C), R24 (D), R48 (E), and R72 (F) wing discs. (**G**) Adult wing with some intervein regions marked by yellow arrowheads. (**H** to **K**) Bs-GFP expression in the intervein regions (yellow arrowheads) in undamaged (H), R24 (I), R48 (J), and R72 (K) wing discs. (**L**) Adult wing with the margin outlined in red and intervein regions marked with yellow arrowheads. (**M** to **P**) E(spl)Mb-CD2 (CD2) expression in the margin (red arrowhead) and intervein regions (yellow arrowheads) in undamaged (M), R24 (N), R48 (O), and R72 (P) wing discs. (**Q**) Adult wing with veins marked by arrowheads: L1 (red), L2 (yellow), L3 (magenta), L4 (white), and L5 (blue). (**R** to **U**) Dl immunostaining in provein cells with arrowheads the same colors as in (Q) in undamaged (R), R24 (S), R48 (T), and R72 (U) wing discs. (**V**) Adult wing with green lines marking the D/V boundary and approximate locations of the Wg IR and OR. (**W** to **Z**) Wg immunostaining in undamaged (W), R24 (X), R48 (Y), and R72 (Z) wing discs. Scale bar, 100 μm.

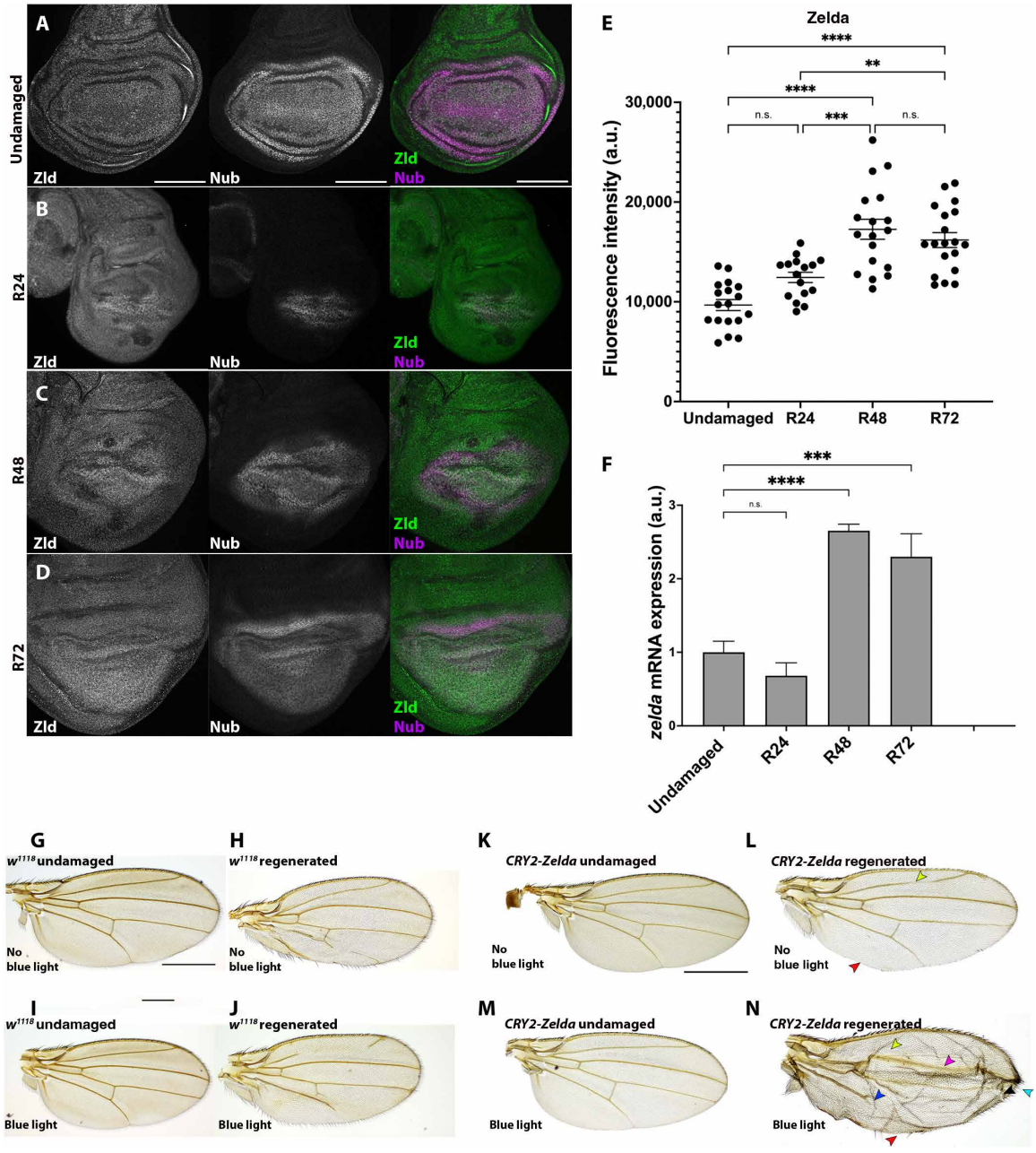

Fig. 2. Zld is important for cell fate and patterning during regeneration. (**A** to **D**) Undamaged (A), R24 (B), R48 (C), and R72 (D) w^{1118} wing discs immunostained for Zld and Nubbin. (**E**) Quantification of Zld immunostaining fluorescence intensity in the Nubbin-expressing wing pouch. $n = 18$ discs each except for R24 ($n = 16$). Undamaged versus R24, $P = 0.0565$ (n.s.); undamaged versus R48, $^{****}P < 0.0001$; undamaged versus R72, $^{****}P < 0.0001$; R24 versus R48, $^{***}P = 0.0002$; R24 versus R72, $^{**}P = 0.0040$; R48 versus R72, $P = 0.7223$ (n.s.); $F = 22.53$, df = 67, one-way analysis of variance (ANOVA) test. a.u., arbitrary units. (**F**) Quantification of *zld* mRNA by qPCR. Undamaged versus R24, $P = 0.9977$ (n.s.); undamaged versus R48, $^{****}P < 0.0001$; undamaged versus R72, $^{***}P = 0.0002$; one-way ANOVA test. (**G** and **H**) Adult wings from w^{1118} animal raised without blue light. (G) Undamaged adult wing. (H) Adult wing from regenerated wing disc. (**I** and **J**) Adult wings from w^{1118} animal raised with blue light. (I) Undamaged adult wing. (J) Adult wing from regenerated wing disc. (**K**) Adult wing from a *CRY2::zld* fly not exposed to blue light. (**L**) Adult wing after disc regeneration in a CRY2::zld fly not exposed to blue light having some defects such as incomplete L2 vein (yellow arrowhead) and incomplete posterior margin (red arrowhead). (**M**) Adult wing from a *CRY2::zld* fly without disc damage exposed to blue light between R0 and R72. (**N**) Adult wing after disc regeneration in a *CRY2::zld* fly exposed to blue light between R0 and R72 having missing L2 vein (yellow arrowhead), altered L3 vein thickness (magenta arrowhead), incomplete L5 vein (blue arrowhead), incomplete posterior margin (red arrowhead), blister formation (black arrowhead), and distal edge vein material (teal arrowhead). Scale bars, 100 μm (wing disc) and 500 μm (adult wing).

the *CRY2::zld* to acute LED blue light led to adult wings that were normal (Fig. 2, G and I). Exposing regenerating discs in w^{1118} larvae to acute LED blue light led to an error rate similar to that of w^{1118} flies that were not exposed to blue light during disc regeneration: 42.3% of wings with minor defects and 12.5% of wings with a strong phenotype for w^{1118} larvae with blue light and 37.8% of wings with minor defects and 17.3% of wings with a strong phenotype for w^{1118} larvae without blue light. Thus, blue light exposure does not cause additional defects during development or regeneration (Fig. 2, H and J, and fig. S1E). In addition, the CRY2 insertion did not interfere with normal wing development (Fig. 2K) or disc regeneration, with defects in adult wings similar to those in w^{1118} controls (Fig. 2, H, J, and L, and fig. S1E). Inactivation of CRY2::Zld by blue light during the third instar did not cause any defects in the adult wing (Fig. 2M), suggesting that Zld is not required for normal wing development. Inactivation of CRY2::Zld throughout larval development, from days 2 to 9 after egg laying, also had no effect (fig. S1D).

Exposing *CRY2::zld* larvae with damaged discs to blue light between R0 and R72 led to 97.24% of adult wings with defects, where 62.84% had minor defects and 34.4% had major defects (Fig. 2N and fig. S1E). Inactivation of Zld during disc regeneration resulted in numerous errors (Figs. 2N; 4, D and E; 6D; and 7E), such as missing or incomplete L2 and L5 veins, altered L3 and L4 vein thickness, missing crossveins, and ectopic vein material at the distal end of the wing. A percentage of each margin was also missing, especially in the posterior portion of the wing (Fig. 2N). Last, these adult wings had a high rate of blisters (Fig. 2N). We observed some variability in the frequency of these defects, likely due to the larvae positioned at different depths in the food, resulting in inequal exposure to blue light. However, the phenotypes observed were consistent and reproducible.

To narrow down the requirement for Zld to early, mid, or late regeneration, we used blue light to inactivate CRY2::Zld between R0 to R24, R24 to R48, and R48 to R72 (fig. S1C). Inactivation of Zld during each of these time windows produced phenotypes similar to inactivation of Zld throughout regeneration (R0 to R72) (fig. S1, F to I). We quantified specific patterning defects in the adult wings, including presence of vein and bristles on the posterior margin (fig. S1J), presence of a blob of vein at the distal end of the wing (fig. S1K), and presence of a blister (fig. S1L), and found that inactivating Zld during each of these 24-hour windows produced these phenotypes but not at the same frequency as inactivating Zld throughout regeneration. Thus, Zld may be required throughout regeneration.

To validate that these defects were due to loss of Zld function, we built a *zld* RNA interference (RNAi) transgene by placing a previously published *zld*-specific RNAi sequence (*15*) under the control of a LexA operator (LexAop) (*44*) to avoid regulation by the $Gal80^{ts}$. The *LexAop zld-RNAi* was expressed using a *pdm2-LexA* driver that is expressed in the wing disc pouch and hinge region (fig. S2A). Expression of the *LexAop zld-RNAi* during normal development in the wing disc reduced Zld levels (fig. S2, B and C) but did not lead to any defects in the adult wing, again indicating that that Zld is not required for normal wing development (fig. S2J). Expression of *zld-RNAi* also reduced Zld levels at R24 (fig. S2, D and E), R48 (fig. S2, F and G), and R72 (fig. S2, H and I). This reduction yielded adult wings with similar defects to the CRY2::Zld system, such as missing and/or incomplete veins, ectopic vein material at the distal edge of the wing, missing margins, and blisters (fig. S2, J to O). Adult wings from *pdm2-LexA;attP2* damaged discs in most cases appeared well formed, with 65% of wings regenerating perfectly ($n = 131$) (fig. S2L). Regenerating discs containing only the *LexAop-zldRNAi* transgene resulted in adult wings with mild defects that were nevertheless similar to those seen with *zld* knockdown during regeneration, suggesting that this *LexAop* promoter might allow leaky expression of the RNAi (fig. S2K). Thus, inactivation of Zld by CRY2 and RNAi-mediated knockdown of *zld* after damage resulted in many patterning and cell fate defects, as well as blistering in the adult wing.

Zld is enriched at developmental genes during mid-regeneration

To identify the genes Zld regulates to facilitate correct regeneration, we performed the protein-DNA binding assay CUT&RUN (*45*) to find where Zld binds throughout the *Drosophila* genome in undamaged and regenerating wing discs at R48. We chose the R48 time point because that was the time of both peak Zld expression and the initiation of patterning gene expression returning to normal. We used flies homozygous for a functional, endogenous Zld tagged with superfolder GFP (*43*) together with a commercially available anti-GFP antibody (Abcam, Ab290). One hundred wing discs were dissected for each replicate from undamaged and R48 larvae, as well as from controls that lacked the GFP::Zld. Data analysis was carried out using standard programs, including deepTools, MACS2, and ChIPSeeker (*46*–*48*).

To estimate the number of genes that may be regulated by Zld, we examined enrichment near transcription start sites (TSSs) (Fig. 3A). Our CUT&RUN data showed that Zld had only 170 binding sites near TSSs in undamaged wing discs (Fig. 3A), consistent with our finding that Zld is dispensable for normal wing development. By contrast, we found that Zld bound near almost 1900 TSSs in mid-regenerating wing discs (Fig. 3A), consistent with our finding that reduction of Zld induced a strong phenotype in wings after disc regeneration. Examining the distribution of the Zld binding sites along genes revealed a marked shift from mostly intergenic regions in undamaged discs to mostly promoter regions in regenerating discs (Fig. 3B). Overall, Zld had 1368 binding sites in the undamaged discs and 3732 binding sites in R48 discs with significantly increased differential binding to its target sites compared to undamaged samples (Fig. 3C and tables S2 and S3).

To determine the extent to which Zld binding in regenerating wing discs is similar to Zld binding in other tissues, we compared the genomic loci bound by Zld during regeneration with previously published chromatin immunoprecipitation sequencing (ChIP-seq) data for Zld during stage 14 of embryonic development (*9*) and in type II neuroblasts of the larval brain (*17*). Notably, there were substantially more Zld-bound loci in embryos (20,119) relative to neuroblasts (7215) and wing discs (3732). However, 69% of the loci bound in regenerating discs were also bound in embryos (fig. S3A). By contrast, only 31% of the loci bound in regenerating discs were also bound in type II neuroblasts (fig. S3A). The lack of greater overlap among the datasets may be due to differential Zld binding in different tissues and/or the different sensitivities of the ChIP-seq and CUT&RUN techniques. Further analysis showed that while 50% of Zld binding sites were within 1 kb of gene promoters in regenerating discs (Fig. 3B), with the remainder in exons, introns, and intergenic regions, neuroblasts had substantially more binding sites near promoters and fewer sites in introns and distal to the genes (fig. S3, B and C).

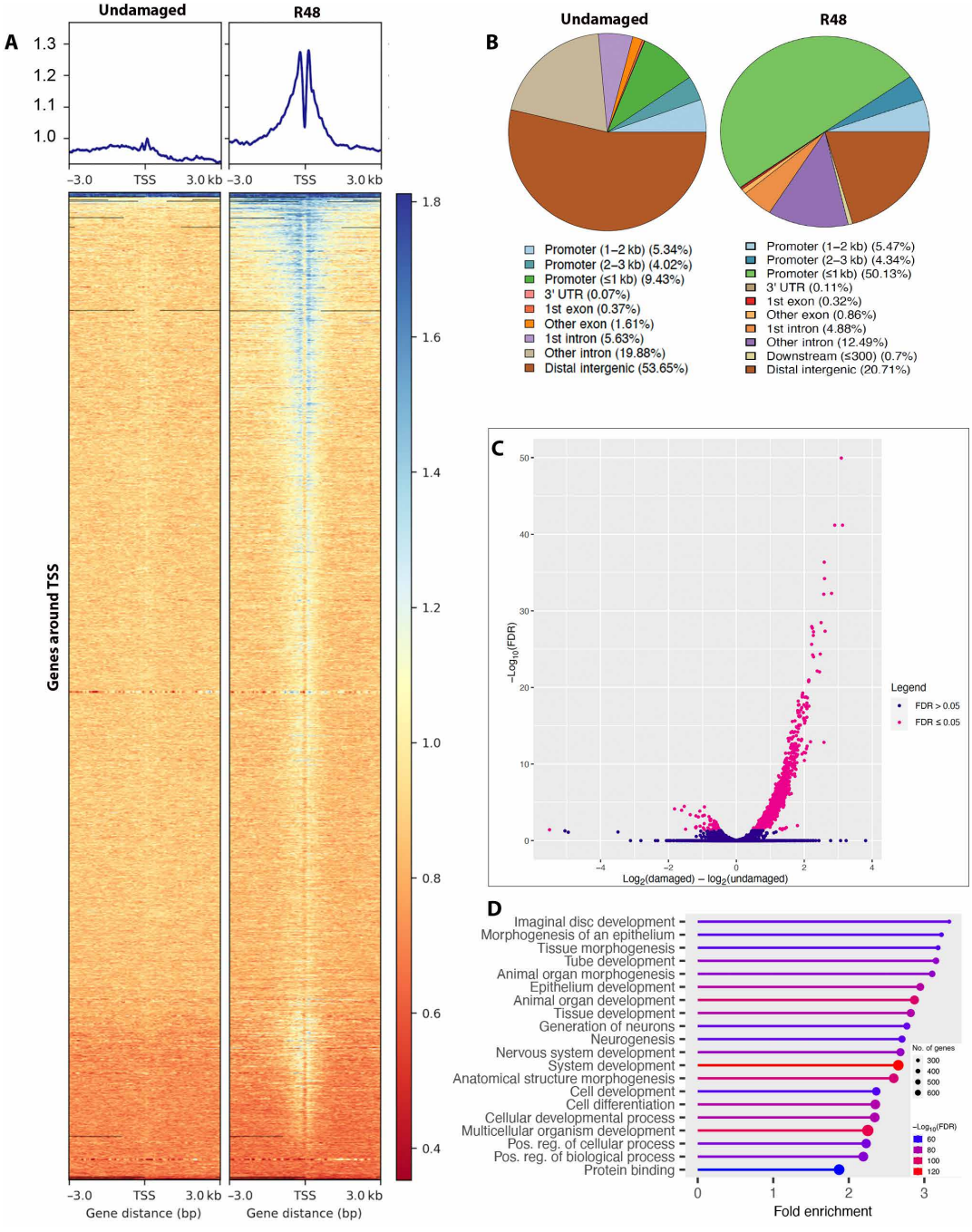

Fig. 3. Zld binds near genes important for wing development and morphogenesis. (**A**) Heatmap of Zld occupancy in undamaged and regenerating wing discs ± 3 kb from TSSs. Each line is an individual gene. Color indicates normalized read counts from high (blue) to low (red). (**B**) Distribution of genomic locations of annotated Zld binding sites relative to genes using ChIPseeker in undamaged and R48 discs. UTR, untranslated region. (**C**) Volcano plot showing differential binding in undamaged versus R48 discs. FDR, false discovery rate. (**D**) Biological processes enriched in the genes near Zld binding sites according to Gene Ontology (GO) analysis.

We assessed the list of genes near Zld binding sites in regenerating wing discs using Gene Ontology (GO) tools. We found enrichment for genes involved in various developmental and morphogenesis processes (Fig. 3D), consistent with the patterning defects observed in wings when Zld was reduced during regeneration. To validate our CUT&RUN data, we assessed expression of genes near putative Zld binding sites individually. One such gene was *fz2*, which encodes a receptor for WNT family ligands such as Wg and is important for developmental processes dependent on WNT signaling (*49*). Zld did not bind near *fz2* in undamaged discs but bound in several locations in R48 discs (fig. S3D). *fz2* also provides an example of the overlap and differences in binding sites among imaginal discs, embryos, and neuroblasts, with three loci bound in all three tissues, one locus bound only in regenerating discs and neuroblasts, five loci bound only in embryos, and one locus bound only in neuroblasts (fig. S3D).

Frizzled2 (Fz2) is expressed in the notum and in the dorsal and ventral regions of the wing pouch (fig. S3E). Inactivation of Zld during normal development did not change Fz2 expression levels or patterning (fig. S3, F and I). During late regeneration, Fz2 was expressed throughout the regenerating pouch at R72 (fig. S3G) and was markedly reduced upon inactivation of Zld (fig. S3, H and I). Thus, we established that a developmental patterning gene near a Zld binding site requires Zld for full expression during regeneration. Hence, we wondered whether Zld could be important for correct expression of other developmental genes during regeneration.

Zld regulates genes important for wing margin and sensory bristle fate

Adult wings that developed from damaged and regenerated discs in which Zld had been inactivated or knocked down had very specific defects in veins, margins, and sensory bristles. Hence, we wondered whether Zld could be responsible for inducing expression of specific genes required for these cell fates. First, we confirmed that inactivation or knockdown of Zld during normal development did not lead to any vein disruption in adult wings, defects in the wing margin, or loss of sensory bristles on the anterior margin (Fig. 4, A and B, and fig. S4A). In addition, adult wings formed from regenerating control wing discs that either had the CRY2 insertion but regenerated without blue light exposure or had the genotype *pdm2-LexA/+;attP2/+* were well patterned, with occasional disruption of veins and margins when patterning defects were quantified (Fig. 4C and fig. S4, B and D to H).

Last, we analyzed adult wings that arose from wing discs that regenerated while Zld was inactivated or knocked down. Quantitative analysis demonstrated a high percentage of these wings had errors including poorly defined L3 and L4 veins and margin missing in sections along with absent sensory bristles on the anterior side (Fig. 4D and fig. S4, C and D). In addition, large sections of the L2 and L5 veins were missing (Fig. 4, D and E, and fig. S4, C to E), and anterior and posterior crossveins were missing (fig. S4, C, F, and G). These wings also had aberrant vein tissue on the distal edge of the adult wing (Fig. 4D and fig. S4H) and had substantial sections of margin missing on the posterior edge (Fig. 4, E and F, and fig. S4C). Thus, Zld appears to be crucial for vein and margin cell fate specification during disc regeneration.

To understand how Zld is regulating these cell fates, we asked whether Zld binds near genes important for margin and vein identity using our CUT&RUN data. First, we looked for genes near Zld binding sites that are important for margin fate. At R48, Zld is bound at the promoter region of *ct* (fig. S4I), which is expressed in the D/V boundary of developing wing discs and is important for margin fate (Fig. 1, B and C) (*25*, *26*, *50*). Ct expression along the D/V boundary remained stable upon Zld inactivation during normal development, as expected (Fig. 4, G and H). As previously shown, Ct expression was lost during regeneration and reappeared by R72 (Fig. 1, B to F). On average, Ct was expressed in 87% of the D/V boundary by R72 (Fig. 4, I and K), indicating restoration of most of the margin. The gaps in Ct expression were likely responsible for the sporadic sections of margin missing in the resulting adult wings (Fig. 4F). After Zld inactivation, R72 discs had variable expression of Ct, with some discs missing over 90% of Ct expression (Fig. 4J). On average, only 57% of the D/V boundary expressed Ct by R72 (Fig. 4K), which correlated with the high percentage of the adult wing margin missing after regeneration in wing discs lacking functional Zld.

We also looked for genes near Zld binding sites that are important for vein identity. Zld bound at the promoter and intronic regions of Dl (fig. S4J), which is expressed in the provein cells in developing wing discs and is important for provein fate and consequently intervein fate (*29*, *51*). There was no difference in Dl expression between undamaged discs with and without functional Zld (Fig. 4, L and M). As previously shown, Dl expression transitioned from a thin stripe at R24 to a broader and more diffused signal at R48 (Fig. 1, S and T). However, upon Zld inactivation, R48 discs had a markedly reduced Dl signal (fig. S4, K to M), suggesting that Dl is a target of Zld. Furthermore, while Dl expression in control regenerating discs at R72 had mostly returned to normal, with L2 and some L5 provein cells missing Dl expression in a few discs (Fig. 4N), 64% of R72 discs that lacked Zld function had incomplete expression of Dl (Fig. 4O). The errors included L2 and L5 proveins lacking expression and weak expression in the L3 and L4 proveins (Fig. 4O). Dl was also expressed diffusely in between the presumptive L3 and L4 proveins (Fig. 4O), which is the region that gives rise to the tip of the wing and thus could be responsible for the extra vein material on the distal edge of the wing (Fig. 4D and figs. S2O and S4C).

Tracts of sensory bristles were also often missing along the anterior margin of the wing after disc regeneration without Zld (Fig. 4, A to D). Expression of the transcription factor *achaete* (*ac*) is crucial for sensory bristle development (*52*) and was identified as a putative target of Zld at R48 in our CUT&RUN analysis (fig. S4N). During normal development, Ac-expressing cells are found in the anterior half of the wing disc flanking the D/V boundary (Fig. 4P) and are unaffected upon Zld inactivation (Fig. 4Q). In R72 regenerating discs, Ac-expressing cells were present as expected (Fig. 5R). However, in R72 discs that lacked Zld (Fig. 4, S to U), 38% had few Ac^+ cells (Fig. 4S), 31% had a reduced number of Ac^+ cells (Fig. 4T), and 31% had evenly distributed Ac^+ cells in the anterior compartment (Fig. 4U). This loss of Ac correlated with absent sensory bristles in the adult wing. We also saw a percentage of wings with aberrant Ac expression on the posterior side of the wing disc (Fig. 4, T and U), suggesting that Zld may play a role in maintaining proper posterior fate during regeneration. Together, our results show that Zld is important for the reestablishment of margin, sensory bristle, and vein fates in the regenerating wing disc by regulating expression of targets such as *ct*, *ac,* and *Dl*, respectively.

Loss of Zld delays the transition to normal patterning in regenerating wing discs

We wondered whether Zld's regulation of targets during mid to late regeneration is an integral aspect of the transition from regeneration

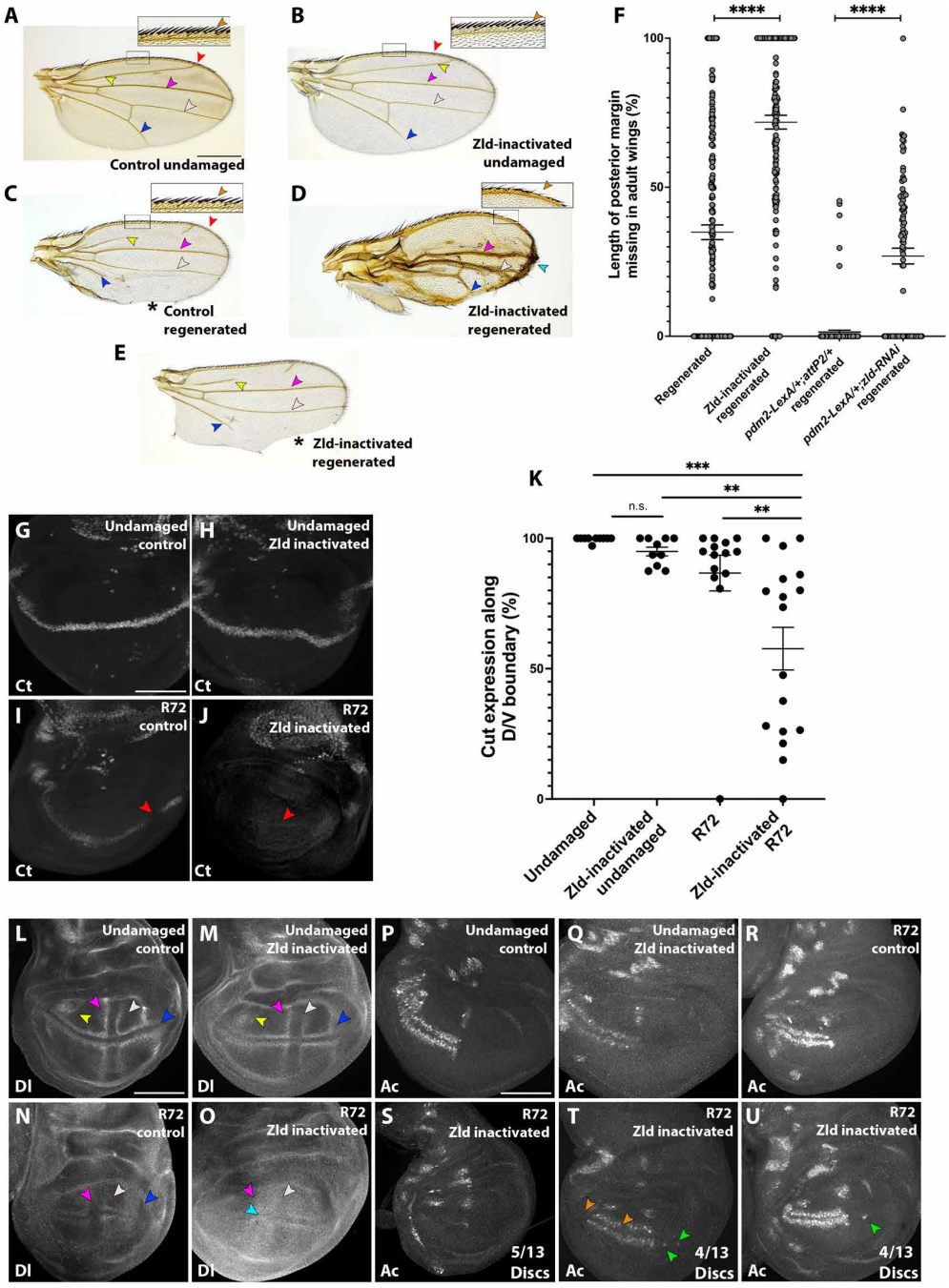

Fig. 4. Zld regulates margin, vein, and sensory organ fate after regeneration. (**A**) Undamaged adult wing showing L1 (red arrowhead), L2 (yellow arrowhead), L3 (magenta arrowhead), L4 (white arrowhead), and L5 (blue arrowhead) veins and sensory bristles (orange arrowhead; with higher magnification inset). (**B**) Adult wing after Zld inactivation during normal development, arrowheads as in (A). (**C**) Adult wing after disc regeneration, arrowheads as in (A). (**D** and **E**) Adult wings after Zld inactivation during regeneration, arrowheads as in (A). Asterisk (*) indicates missing posterior margin. (**F**) Quantification of missing posterior margin for control wings after regeneration ($n = 207$), Zld-inactivated wings after regeneration ($n = 190$), control *pdm2-LexA;attP2/+* RNAi wings after regeneration ($n = 131$), and *pdm2-LexA;zld-RNAi/+* wings after regeneration ($n = 91$). $^{****}P < 0.0001$, Student's *t* test. Controls of the same genetic background were used for comparison due to variation in background error rates in patterning. (**G** to **K**) Ct immunostaining in an undamaged wing disc (G), undamaged disc with Zld inactivation (H), R72 wing disc (I), R72 wing disc with Zld inactivation (J), and quantification of cut expression along D/V boundary (K) for undamaged discs: control ($n = 10$), Zld inactivated ($n = 10$), and R72 discs for control ($n = 14$) and Zld inactivated ($n = 17$). Undamaged versus Zld-inactivated undamaged, $P = 0.972$ (n.s.); undamaged versus Zld-inactivated R72, $^{***}P = 0.0003$; Zld-inactivated undamaged versus Zld-inactivated R72, $^{**}P = 0.0017$; R72 versus Zld-inactivated R72, $^{**}P = 0.0083$; one-way ANOVA (K). (**L** to **O**) Dl immunostaining in an undamaged wing disc (L), undamaged wing disc with Zld inactivation (M), R72 regenerating wing disc (N), and R72 regenerating wing disc with Zld inactivation (O). Arrowheads mark L2 (yellow), L3 (magenta), L4 (white), and L5 (blue). (**P** to **U**) Ac immunostaining in an undamaged wing disc (P), undamaged wing disc with Zld inactivation (Q), R72 wing disc (R), and R72 wing disc with Zld inactivated (S to U). Scale bars, 500 μm (adult wings) and 100 μm (all discs).

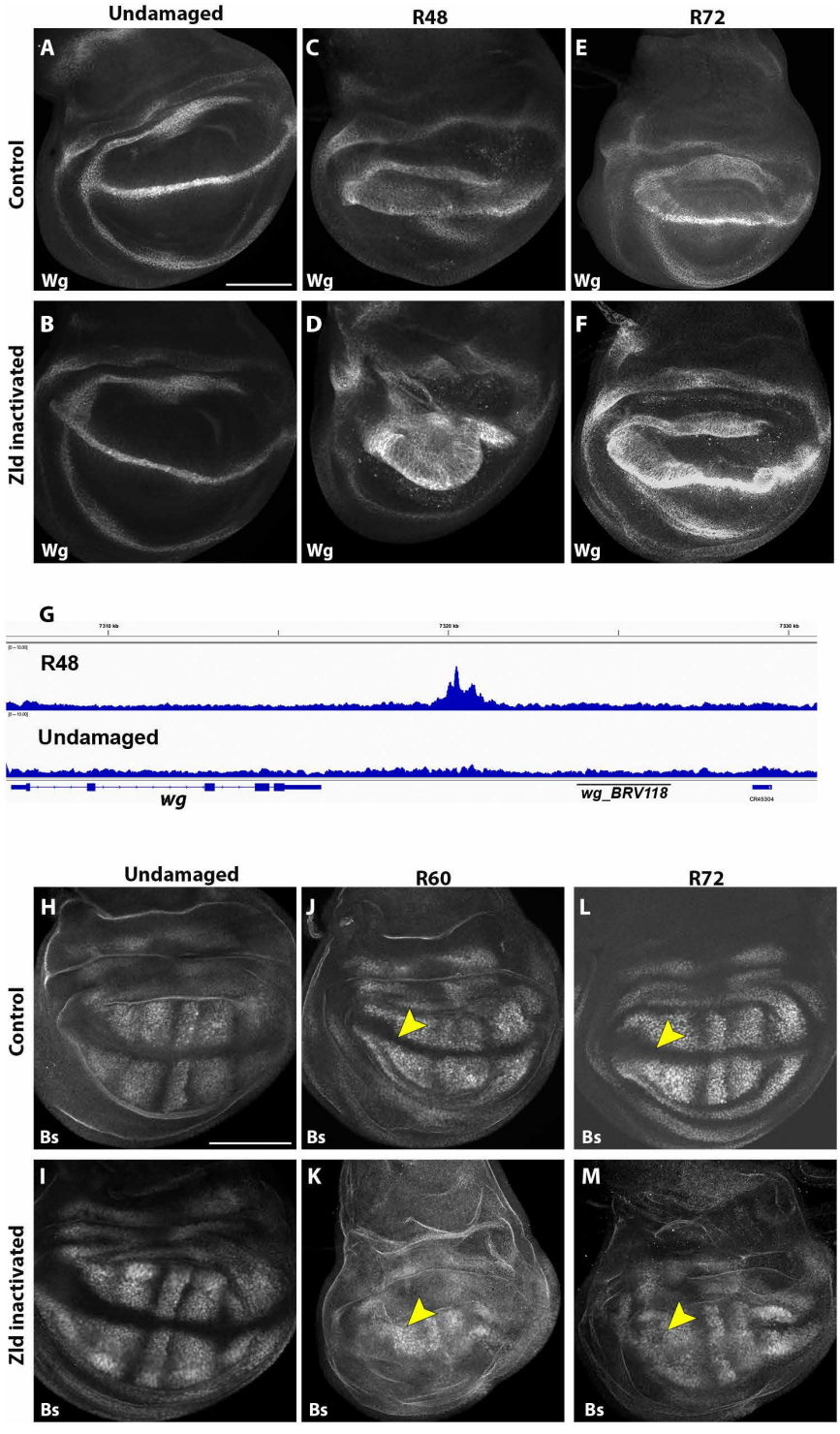

Fig. 5. Zld regulates timely patterning transitions during regeneration. (**A** to **F**) Wg immunostaining in an undamaged disc (A), undamaged disc with Zld inactivated (B), regenerating disc at R48 (C), R48 regenerating disc with Zld inactivation (D), regenerating disc at R72 (E), and R72 regenerating disc with Zld inactivation (F). (**G**) Region bound by Zld near Wg from CUT&RUN data in undamaged and R48 discs. Note that the binding site is distinct from the damage-responsive *BRV118* enhancer and the developmental *wg*[1] enhancer. (**H** to **M**) Bs immunostaining in an undamaged disc (H), undamaged disc with Zld inactivated (I), regenerating disc at R60 (J), R60 regenerating disc with Zld inactivation (K), regenerating disc at R72 (L), and regenerating disc at R72 with Zld inactivated (M). Scale bars, 100 μm (all discs).

back to normal development (Fig. 1, C to F and R to U). Wg and Bs are expressed in complex patterns in the third instar wing disc, which are established by the integration of many other signals and patterned expression of transcription factors (Fig. 1, H and W) (*27*, *53*). In addition, those complex expression patterns are lost as signaling centers and patterning reorganizes during regeneration and is regained after most regenerative growth has occurred (Fig. 1, H to K and W to Z) (*7*, *8*). Thus, we used Wg and Bs patterning as general readouts for the patterning state of the disc to elucidate the extent to which Zld is important for facilitating timely transitions during regeneration.

To determine the extent to which Zld is important for the mid-regeneration transition to the normal Wg expression pattern (Fig. 1Y), we examined Wg expression while inactivating Zld. During normal development, inactivation of Zld did not alter Wg expression (Fig. 5, A and B). During regeneration of control discs at R48, Wg expression was transitioning to its normal expression at the D/V boundary and the inner and outer hinge rings in all but 15.3% of discs (Fig. 5C). However, when we inactivated Zld during regeneration, 48% of wing discs retained Wg expression throughout the pouch at R48, appearing similar to R24 wing discs (Figs. 1X and 5D). By R72, 73% of control wing discs had returned to the normal Wg expression pattern (Fig. 5E), while 67% of R72 wing discs with Zld inactivation still had thicker stripes of expression and an incomplete IR (Fig. 5F). Thus, reducing Zld compromised the timely transition of Wg expression during mid-regeneration in a large percentage of regenerating discs.

We wondered whether this prolonged ubiquitous expression of Wg in regenerating discs upon Zld inactivation had any impact on regenerative growth. Unexpectedly, Zld inactivation resulted in a higher percentage of fully regenerated wings (75 to 100% wing size) (fig. S5, A to E), although they had many patterning defects. To determine whether the improved wing size was due to persistence of elevated proliferation after R48 due to continued Wg signaling, we measured both pouch size and mitoses throughout regeneration. The regenerating wing pouches that lacked Zld function were already larger than controls by R48 (fig. S5, F to J), indicating that the regenerative advantage occurred before the extended time of elevated Wg expression. We observed an increase in mitoses at R24 but not at R48 (fig. S5, K to O), which could explain the larger pouch by R48. Thus, the sustained Wg expression at R48 in discs with inactivated Zld did not appear to enhance proliferation in mid-regeneration. However, these data suggest that Zld may constrain proliferation during early wing disc regeneration and identification of how Zld restricts regenerative growth will be of interest in future studies.

We wondered whether the effect of loss of Zld on the transition back to the normal expression pattern of Wg was due to direct regulation of the developmental and regeneration enhancers that control Wg expression, or regulation of uncharacterized Wg enhancers, or due to an indirect effect on general patterning. Wg expression during disc development and regeneration is regulated by the wg^{1} and *BRV118* enhancers in the *wg-wnt6* regulatory region (*54*, *55*). However, during regeneration, Zld was bound to a region in the *wg-wnt6* regulatory locus (chr2L:7319693 to 7321007) that is outside of the wg^{1} and *BRV118* enhancer region (Fig. 5G). Thus, Zld does not appear to directly act at the wg^{1} and *BRV118* locus. The effect of Zld on the change in Wg patterning may be direct through this uncharacterized enhancer or may be indirect.

To confirm the extent to which the timing of repatterning was disrupted when Zld was lost, we next assessed the transition of Bs expression back to normal. There were no Zld binding sites near *Bs* at R48, so the effects of loss of Zld on Bs expression reflect the overall state of patterning in the regenerating tissue. Bs was barely expressed in the regenerating pouch at R48 (Fig. 1J) but returned to its normal expression at R72 (Fig. 1K). Hence, we examined the intermediate time point of R60. Inactivating Zld in undamaged wing discs had no effect on Bs expression (Fig. 5, H and I). In control R60 regenerating discs, Bs expression was emerging in the intervein regions, was starting to retreat from the proveins, and was excluded from the D/V boundary in 67% of discs ($n = 12$) (Fig. 5J), while the remaining discs had variable Bs expression in the D/V boundary and provein regions. After inactivating Zld, Bs was misexpressed throughout the regenerating pouch at R60, including in the proveins and the D/V boundary in 73% of discs ($n = 11$) (Fig. 5K). While Bs expression had returned to its normal developmental pattern by R72 in 75% of control discs ($n = 8$) (Fig. 5L), 57% ($n = 7$) of Zld-inactivated R72 discs had not transitioned correctly, with haphazard Bs expression, especially along the D/V boundary of the wing disc (Fig. 5M). Thus, Zld appears crucial for the timely transition to normal developmental gene expression patterns during mid to late regeneration, as assessed by Wg and Bs expression.

To determine the extent to which overexpressing Zld during regeneration might promote the premature return of normal patterning, we expressed Zld under UAS control, which drove Zld expression in the remaining rnGAL4-expressing cells and immunostained for Wg (fig. S6, A, B, D, and E). The overexpression of Zld in this subset of cells had the effect of inhibiting regeneration, as Wg expression was reduced at R24 (fig. S6, A to C) and the Wg-expressing area remained significantly smaller than in control discs through R48 (fig. S6, D to F). This poor regenerative response obscured any effects on patterning and was consistent with the finding that reduction of Zld led to enhanced regeneration.

Zld is important for preserving posterior cell fate

We previously showed that the posterior cell fate gene *engrailed* (*en*) is misregulated by JNK signaling during regeneration, which induces overexpression, followed by autoregulated silencing of *en* (*38*). To prevent this misregulation, the SERTAD [SERTA (SEI-1, RBT-1, and Tara) Domain containing] ortholog *taranis* (*tara*) and the SWI/SNF (SWItch/Sucrose Non-Fermentable) BAP (Brahma-associated Protein) complex, defined by the BAP-specific complex member *osa*, act as protective factors to prevent *en* overexpression (*37*, *38*). While *tara* expression is activated in late regeneration, how its expression is activated and how *osa* activity is regulated are not known. Reduction of either *tara* or *osa* during normal development does not cause adult wing defects (fig. S7, A, C, and E), but their reduction during regeneration leads to adult wings that have a number of anterior features on the posterior half of the wing, namely, vein material on the posterior margin, sensory bristles on the posterior margin, an extra anterior crossvein on the posterior side, anterior compartment shape in the posterior compartment, and distal costa bristles on the posterior side (fig. S7, B, D, and F) (*37*, *38*). These defects are collectively called P-to-A transformations. We noticed that the anterior marker Ac was often misexpressed in the posterior compartment of regenerating discs during Zld inactivation (Fig. 4, T and U), suggesting that P-to-A transformations were taking place.

To generally assess the effects of loss of Zld on posterior cell fate, we examined adult wings. Loss of Zld did not affect posterior cell fate during normal development (Fig. 6, A and B). Adult wings after disc regeneration had occasional P-to-A transformations, with sporadic anterior sensory bristles and vein material on the posterior margin, as seen previously (Fig. 6C) (*37*, *38*). However, adult wings after regeneration with Zld inactivation or knockdown had a much higher frequency of P-to-A transformations, including vein material and sensory bristles on the posterior margin, and extra anterior crossveins on the posterior side (Fig. 6D and fig. S7H). However, these wings were also often missing large sections of the posterior margin and were missing many or all veins (Fig. 4, E and F). Thus, we could not quantitate frequency of sensory bristles and vein material on the posterior margin due to the frequent absence of the posterior margin itself, nor could we quantitate frequency of a second anterior crossvein in wings that often lacked all veins.

To confirm that the phenotypes observed in the adult wings were due to P-to-A transformations during disc regeneration, we immunostained for the Hedgehog receptor Patched (Ptc). Ptc is expressed in the anterior cells near the anterior-posterior boundary and during regeneration that expression remained restricted to the anterior side of the anterior-posterior boundary (Fig. 6, E and F). By contrast, R72 discs that lacked Zld function had Ptc expression in the posterior compartment (Fig. 6G), indicating posterior cells that were attaining anterior fate. We also immunostained for the posterior selector transcription factor En, whose misregulation during regeneration is enhanced when levels of the protective factors *tara* or *osa* are reduced (*37*, *38*) (fig. S7, I to P). Similarly, when Zld was inactivated in regenerating discs, *en* expression was silenced in portions of the posterior compartment (Fig. 6, H to J). Thus, Zld plays a role in regulating *en* expression during late regeneration to preserve posterior fate.

We wondered whether Zld could help preserve *en* expression by regulating the expression of *tara* or *osa*. Our CUT&RUN analysis showed that Zld binds to sites near *en*, *tara*, and *osa* in regenerating discs (fig. S7, Q and U), raising the possibility of direct and/or indirect regulation of *en* by Zld. Osa protein levels and transcription of *tara* were not altered when Zld was inactivated during normal development (fig. S7, R to T and V to X). In regenerating wing discs, Osa levels were not significantly different between undamaged and control R72 discs (Fig. 6, K and L). However, there was a notable decrease in Osa levels in the regenerating pouch of R72 discs after inactivation of Zld (Fig. 6, L to N). In contrast to *osa*, *tara* expression was significantly up-regulated in mid and late regenerating discs (Fig. 6, O and P) (*38*). Upon Zld inactivation in R48 discs, *tara* transcription as assessed by an enhancer trap was significantly decreased (Fig. 6, P to R). Thus, our results suggest that Zld can regulate posterior fate in part by controlling expression of the protective factors *osa* and *tara* to prevent *en* from being silenced during late regeneration.

To confirm these findings, we tried to rescue the P-to-A defects caused by loss of Zld by overexpressing *tara*. Tara overexpression eliminated the ectopic Ptc expression in the posterior of the disc and largely rescued loss of En in the posterior of the disc, although some discs at R72 still had small areas of En silencing (Fig. 6, S to V). The resulting adult wings had few P-to-A defects, although additional phenotypes such as loss of margin remained (Fig. 6W). Thus, Zld regulates *tara* and *osa*, which prevent loss of posterior fate in late regeneration.

Zld is important for the structural integrity of the adult wing after disc regeneration

Inactivation of Zld during regeneration led to a high frequency of blisters in the adult wings.

There were no blisters after normal development during which Zld was inactivated or knocked down (Fig. 7, A, B, and D). After wing disc regeneration in control animals, about 5% of adult wings had blisters (Fig. 7C). Control *pdm2-LexA/+;attP2/+* regenerated discs also regenerated well, with blisters in only 3% of adult wings after disc regeneration (Fig. 7D). By contrast, after Zld inactivation during disc regeneration, 23% of the adult wings had blisters (Fig. 7, E, G, and H). RNAi-mediated *zld* knockdown during disc regeneration also caused blisters in 33% of adult wings (Fig. 7, F and H). Thus, Zld likely controls expression of genes important for the integrity of the adult wing.

Integrins play an important role in adhesion of the apposed basal layers of the wing disc when undergoing metamorphosis and keep the junctions connected as the wing goes through expansion to unfold the adult wing blade after eclosion (*56*–*58*). Zld was bound near the βPS (beta position-specific) integrin *myospheroid* (*mys*) and αPS1 integrin *multiple edamatous wings* (*mew*) at R48. During normal development, Mys is expressed throughout the wing disc, with slightly elevated levels in the ventral and dorsal regions of the pouch and higher expression at the D/V boundary (Fig. 7K). Inactivation of Zld did not affect Mys expression during normal wing development (Fig. 7L). During regeneration, control R72 discs had elevated expression of Mys compared to normal development, especially at the D/V boundary (Fig. 7M). By contrast, R72 discs in which Zld had been inactivated had reduced expression of Mys with a marked decrease at the D/V boundary (Fig. 7, N and O).

During normal wing development, Mew is expressed in the dorsal and ventral parts of the wing pouch (Fig. 7P) and was not affected upon Zld inactivation (Fig. 7Q). During regeneration, control R72 discs had high expression of Mew, particularly in the ventral part of the pouch, which was notably lost upon Zld inactivation in 68% of R72 discs ($n = 19$) (Fig. 7, R and S). As expression of integrins in both dorsal and ventral halves of the disc is crucial for maintaining junctions and cell adhesion while the disc undergoes apposition and everts, loss of Mys at the D/V boundary and loss of Mew in the ventral half of the disc likely contribute to the observed blisters.

Trl/GAF and Fkh likely act with Zld to regulate patterning after regeneration

To assess the mechanism through which Zld functions in regeneration, we used the sequences that comprise the Zld binding sites during wing disc regeneration to find enriched motifs that might bind Zld or any transcription factors that might regulate the same loci. The pioneering activity of Zld in early embryos is due to its ability to bind to CAGGTAG sequences throughout the genome (*9*), but Zld binds to other sequences in transcriptionally active tissues such as the type II neuroblasts (*17*). One common cofactor for Zld in both tissues is the pioneer factor GAF, encoded by *Trl*, which recognizes GA-rich repeats (*16*, *17*). Zld binding sites in regenerating wing discs at R48 were not enriched for CAGGTAG sites but did contain GA-rich repeats, suggesting that GAF could be acting at the same loci as Zld during wing disc regeneration (Fig. 8A). Zld binding sites were also enriched for motifs that are recognized by other transcription factors, including the pioneer factor Fkh, and motifs recognized by unconfirmed factors, such as CA-rich repeats (Fig. 8A and fig. S8A).

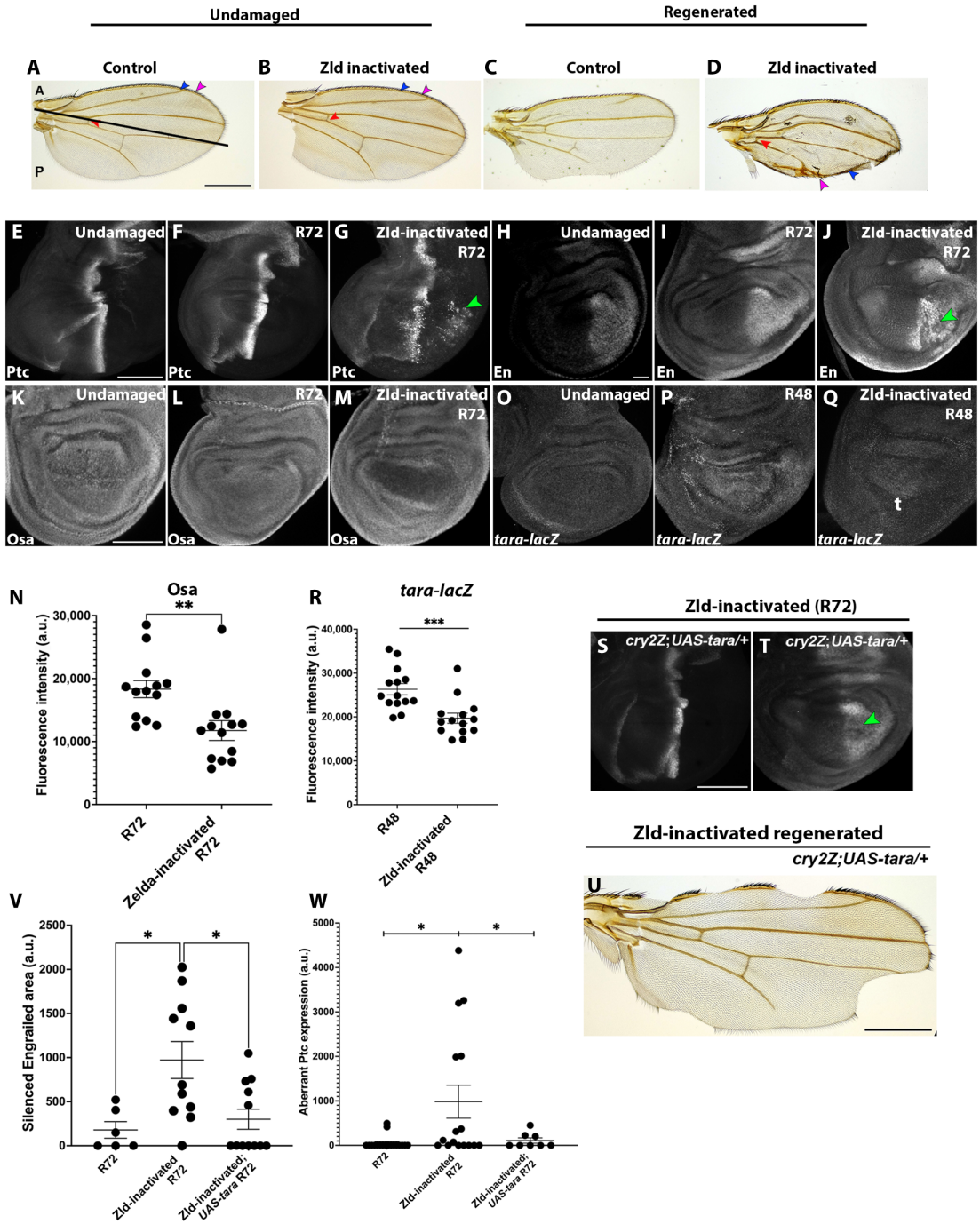

Fig. 6. Zld stabilizes posterior cell fate during late regeneration. (**A** and **B**) Control (A) and Zld-inactivated (B) undamaged adult wings. Blue arrowhead, L1 vein; magenta arrowhead, sensory bristles; red arrowhead, anterior crossvein. (**C** and **D**) Adult wings after disc regeneration, with arrowheads as in (A). (C) Control and (D) Zld inactivated during regeneration. (**E** to **G**) Ptc expression in undamaged (E), R72 control (F), and R72 with Zld-inactivated (G) wing discs. (**H** to **J**) En expression in undamaged (H), R72 control (I), and R72 with Zld-inactivated (J) wing discs. (**K** to **M**) Osa expression in undamaged (K), R72 control (L), and R72 with Zld-inactivated (M) wing discs. (**N**) Quantification of Osa levels in regenerating tissue ($n = 13$ for all). R72 versus Zld-inactivated R72, $^{**}P = 0.0044$; Student's t test. (**O** to **R**) *tara-lacZ* expression in undamaged (O), R48 control (P), and R48 with Zld-inactivated (Q) wing discs. (R) Quantification of *tara*-lacZ in regenerating tissue ($n = 14$ for all). R48 versus Zld-inactivated R48, $^{***}P = 0.0007$; Student's t test. (**S**) Ptc expression in an R72 disc with Tara overexpression and Zld inactivation. (**T**) En expression in an R72 disc with Tara overexpressed and Zld inactivated. (**U**) Adult wing from regenerated wing disc with Tara overexpression and Zld inactivation. (**V**) Quantification for En silencing in control R72 discs ($n = 6$), Zld-inactivated R72 discs ($n = 11$), and Zld-inactivated R72 discs with Tara overexpression ($n = 11$). R72 versus Zld-inactivated R72, $^{*}P = 0.0138$. Zld-inactivated R72 versus Zld inactivated; UAS-tara R72, $^{*}P = 0.0111$; one-way ANOVA. (**W**) Quantification of aberrant Ptc expression in control R72 discs ($n = 18$), Zld-inactivated R72 discs ($n = 16$), and Zld-inactivated R72 discs with Tara overexpression ($n = 9$). R72 versus Zld-inactivated R72, $^{*}P = 0.0136$. Zld-inactivated R72 versus Zld inactivated; UAS-tara R72, $^{*}P = 0.0413$; one-way ANOVA. Scale bars, 500 μm (adult wings) and 100 μm (all discs).

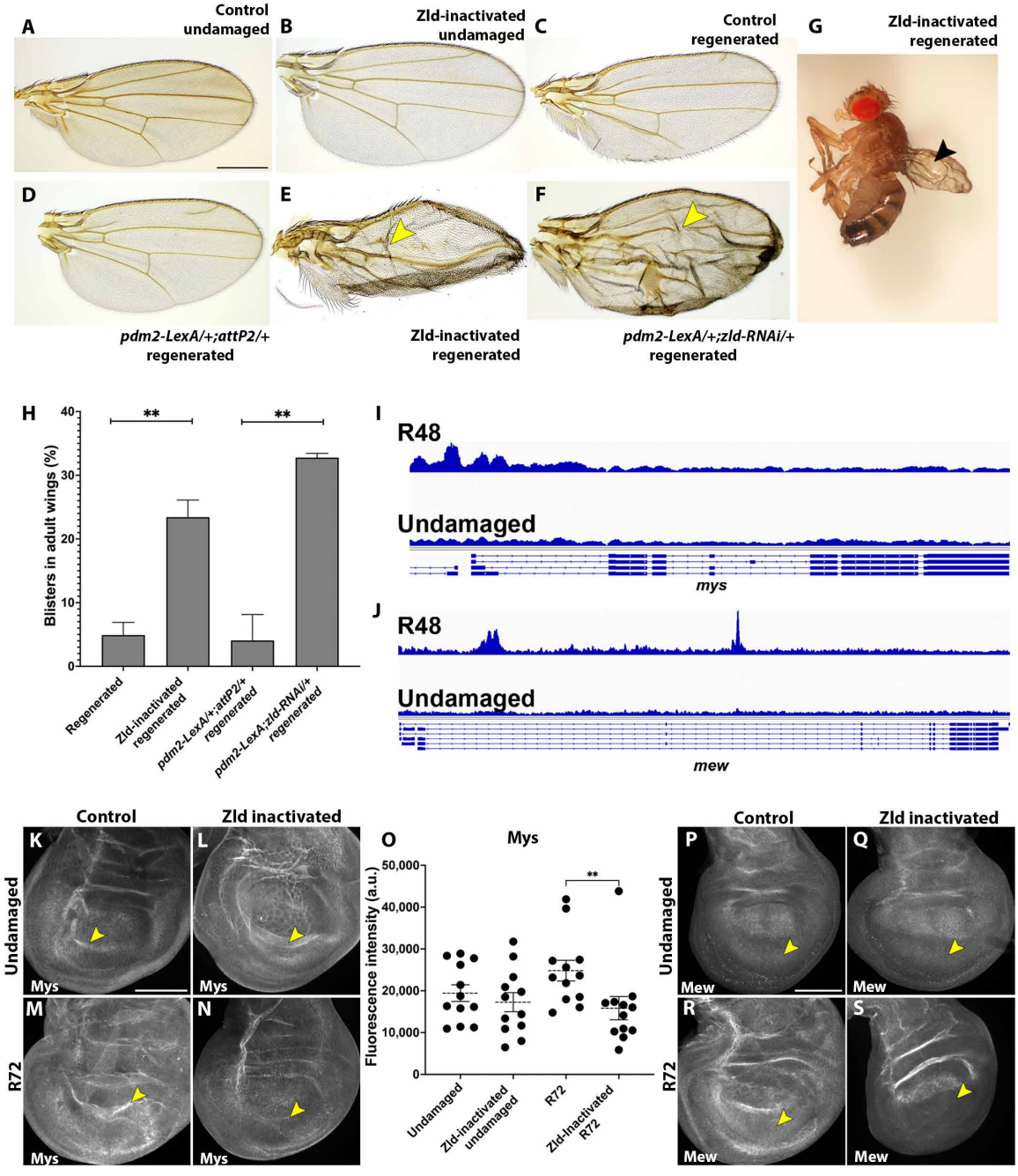

Fig. 7. Zld prevents blisters in the adult wing after disc regeneration. (**A** and **B**) Normal adult wing, control (A) and after Zld inactivation (B). (**C** and **D**) Adult wing after regeneration of a control disc (C) and from *pdm2-LexA/+;attP2/+* control disc (D). (**E**) Adult fly after disc regeneration with Zld inactivation. Yellow arrowhead indicates blister. (**F**) Adult wing after disc regeneration with RNAi-mediated *zld* knockdown. Yellow arrowhead indicates blister. (**G**) Three-dimensional image of a fly with regenerated adult wing after larval damage with Zld inactivation. Black arrowhead indicates Bs wing. (**H**) Quantification of blisters in adult wings in control (n = 207), Zld-inactivated (n = 190), *pdm2-LexA;attP2/+* RNAi control (n = 131), and *pdm2-LexA;zld-RNAi/+* (n = 91) wings after disc regeneration, $^{**}P < 0.01$; Student's t test. (**I** and **J**) Regions bound by Zld near *mys* (I) and *mew* (J) from CUT&RUN analysis. (**K** and **L**) Mys expression in undamaged wing discs, with elevated Mys at the D/V boundary (yellow arrowhead). Control (K) and Zld inactivated (L). (**M** and **N**) Mys expression in R72 discs with yellow arrowhead pointing to the D/V boundary. Control (M), Zld inactivated (N). (**O**) Quantification of Mys expression, R72 versus Zld-inactivated R72, $^{**}P = 0.0045$; exact P value, Student's t test. (**P** to **S**) Mew expression in wing discs, with yellow arrowhead indicating expression in the ventral half. Undamaged control (P), undamaged with Zld inactivated (Q), R72 control (R), R72 with Zld inactivation (S). Scale bars, 500 μm (adult wings) and 100 μm (all discs).

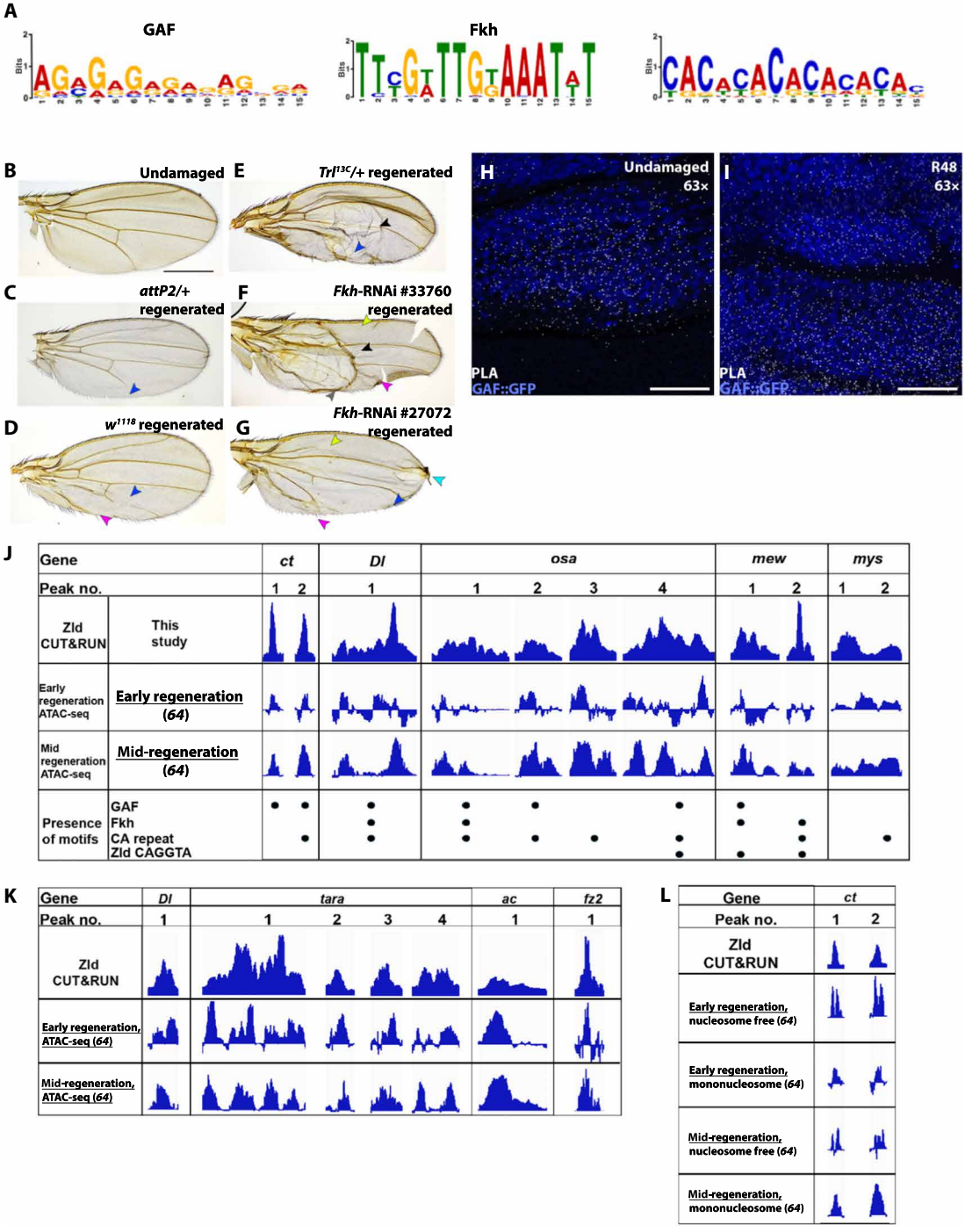

Fig. 8. GAF and Fkh also regulate patterning after regeneration. (**A**) Motif discovery and enrichment analysis of sequences bound by Zld at R48. Enriched motifs were GAF (MEME, $E = 5.3 \times 10^{-24}$), Fkh (MEME, $E = 1.4 \times 10^{-46}$), and CA-rich repeats (MEME, $E = 6.2 \times 10^{-4}$). (**B**) Undamaged adult wings. (**C** to **G**) Adult wings after regeneration for RNAi *attP2*/+ control (C), w^{1118}/+ control (D), Trl^{13C}/+ (E), Fkh-RNAi #27072 (F), and Fkh-RNAi #33760 (G). Arrowheads indicate incomplete L2 vein (yellow), incomplete L5 vein (blue), anterior vein on posterior margin (gray), anterior bristles on posterior margin (pink), extra vein material on distal edge of wing (teal), and blister formation (black). (**H** and **I**) Confocal images taken with a 63× oil objective of the proximity labeling assay (PLA) using antibodies against Zld and GAF-GFP in undamaged (H) and R48 (I) wing discs. PLA is white and the GAF-GFP in the nuclei is blue. Scale bars, 50 μm. (**J**) Chart showing regions of relative chromatin accessibility increases between early (R0) and mid (R15) regeneration aligned with Zld mid-regeneration CUT&RUN data. Dots indicate the presence of GAF/Fkh/CA repeat/Zld motifs at the specified genomic regions. (**K**) Unchanged chromatin accessibility between early (R0) and mid (R15) regeneration aligned with Zld mid-regeneration (R48) CUT&RUN data. (**L**) Accessible regions from ATAC-seq data with nucleosome-length sequenced included (nucleosome) and with nucleosome-length sequences removed (nucleosome-free) near two alternative TSSs for *ct*, aligned with Zld CUT&RUN data. All data ranges for ATAC-seq data are from −48.0 to 120. Data range for Zld R48 track is 0 to 18. Scale bars, 500 μm (adult wings) and 50 μm (wing discs).

We examined adult wings after disc regeneration in animals that were heterozygous mutant for Trl^{13C} or expressed one of two RNAi constructs targeting *fkh* (#33760 and #27072) during regeneration, and each showed phenotypes notably similar, although not identical, to reduction of Zld (Fig. 8, B to G). These phenotypes included P-to-A cell fate changes such as veins and bristles on the posterior edge, extra vein material on the distal edge of the wing, and blisters (Fig. 8, B to G). Results showed the adult wings from the heterozygous mutant Trl^{13C} had a higher rate of P-to-A cell fate changes than the *fkh-RNAi* lines, while knocking down Fkh resulted in more distal edge vein defects and blistering (fig. S8, B to D). It is possible that GAF and Fkh may have different targets during regeneration, as most GAF motifs were near promoters and the Fkh motifs were evenly divided between promoters and intergenic regions (fig. S8, E and F). In addition, the RNAi lines may not knocked down Fkh completely during late regeneration, when posterior fate is more susceptible to misregulation. One RNAi line (#33760) had more severe defects than the other (#27072), which could be due to variance in strength of the knockdown of Fkh. In addition, one RNAi line (#33760) line produced wings with an elongated shape (Fig. 8F), which was not observed with Zld impairment, suggesting that the regeneration-specific targets of Fkh may not completely overlap with those of Zld.

Given that GAF binding motifs were identified in many Zld-bound genomic regions and reduction of GAF gave the same phenotype as reduction of Zld, we wondered whether they could be coordinating to regulate late regeneration genes. GAF and Zld coordinate or function sequentially at the same loci in embryos, although they are not required for each other to bind to chromatin (*13*, *16*) and the GAF binding motif is enriched at Zld-bound loci in neuroblasts (*17*). We asked whether Zld and GAF could be found in the same place at the same time in regenerating discs using the Duolink Proximity Ligation Assay (PLA) (Sigma-Aldrich), which detects instances when two proteins are within 40 nm of each other using protein-specific antibodies and secondary antibodies fused to oligonucleotides that undergo amplification and generate a fluorescent signal when near each other (*59*). We first optimized the PLA for wing imaginal discs and demonstrated that there was no signal in the absence of primary antibodies (fig. S8G) and no signal when antibodies to transcription factors that do not bind each other, En and Pangolin, were used (fig. S8H). By contrast, antibodies to transcription factors known to bind to each other, such as Pangolin/drosophila T-Cell Factor (dTCF) and Groucho (*60*) or Pangolin/dTCF and Armadillo (Arm)/β-catenin (*61*), did produce signal (fig. S8, I and J). To determine whether there are differences in PLA signal between undamaged and regenerating discs, given the increased epithelial permeability of the damaged tissue (*62*), we carried out PLA using two antibodies against the same protein, anti-Arm and anti-GFP in an Arm-GFP fly line. We did not observe a significant difference in the number of PLA foci comparing undamaged and regenerating wing discs (fig. S9, A to C).

Using this technique, we detected PLA signal, indicating proximity, between Zld and GAF using the anti-Zld antibody and a GFP-tagged GAF with an anti-GFP antibody in both undamaged discs and R48 discs (Fig. 8, H and I), with no significant difference in the number of foci between undamaged and regenerating discs (fig. S9D). Thus, Zld and GAF are found in the same place and time in the wing disc, consistent with the enrichment of GAF motifs in the Zld-bound loci in regenerating discs.

To determine the extent to which the regions that are bound by Zld and that contain binding sites for GAF, Fkh, and CA-rich repeats may be changing in accessibility over the course of regeneration, we examined published ATAC-seq datasets from imaginal disc regeneration (*63*, *64*). One of these datasets, in Vizcaya-Molina *et al.* (*64*), examined accessibility across time points during regeneration. However, there were a few differences in the way this study induced damage relative to the current study. Specifically, the damage system used for ATAC-seq ablated less of the disc, by causing ablation in the region that expresses *spalt-major* (*salm*). Therefore, regeneration took less time, so the reported time points of early regeneration (R0), mid-regeneration (R15), and late regeneration (R25) were not the same as those in this study (R0 to R24 for early regeneration, R48 for mid-regeneration, and R72 for late regeneration). To determine whether Zld is also up-regulated when damage is induced in the *salm*-expressing region, we induced ablation with Reaper (Rpr) using the *salm-GAL4* driver for the same amount of time. Zld levels were increased around the damage site at R15, the mid-regeneration time point that is equivalent to R48 in the current study (fig. S9, A to C). Therefore, we examined changes in chromatin accessibility using this ATAC-seq dataset.

We found that many of the regions, but not all, bound by Zld near verified targets had increases in chromatin accessibility between early and mid-regeneration in this ATAC-seq dataset. When comparing accessibility in regenerating discs relative to undamaged discs, Zld-bound regions near *Dl*, *osa*, *ct*, *mew*, *mys*, *wg*, and *fz2* increased in accessibility between early and mid-regeneration (Fig. 8J and fig. S9, D to H). These regions contained binding motifs for GAF and Fkh as well as the CA-rich repeat, but they did not each have all of the motifs (Fig. 8J). While none of them had the canonical CAGGTAG embryonic Zld motif, recent work has used deep learning tools to identify the low-affinity motifs CAGGTA and TAGGTAG, which are also associated with increased chromatin accessibility (*65*). We searched for enrichment of these low-affinity motifs in the Zld-bound regions using MEME Suite and found no enrichment above background (353 sites for CAGGTAG, 328 sites for CAGGTAH, and 363 sites for TAGGTAG). Some of the regions near the validated targets that increase in accessibility contained these low-affinity motifs, but most did not (Fig. 8J), indicating that Zld may bind to as-yet unfound sequences as it does in the neuroblast (*17*). Therefore, Zld may regulate these genes by increasing chromatin accessibility at some of its binding sites over the course of regeneration, allowing the reestablishment of developmental patterning gene expression between mid and late regeneration. Chromatin accessibility at some Zld-bound regions near *Dl*, *tara*, *ac*, and *fz2* remained unchanged (Fig. 8K), suggesting that Zld may not act as a pioneer factor at all loci or other redundant factors may be present, consistent with findings in the embryo (*9*). Given the very similar phenotypes obtained when GAF and Fkh were reduced (Fig. 8, B to G), these pioneering transcription factors may also contribute to changes in accessibility or transcription activation.

Many of the Zld-bound regions were near TSSs, where single nucleosomes regulate access to promoter regions (*66*). ATAC-seq fragmentation can generate small fragments in open chromatin regions and fragments the size of mononucleosomes and dinucleosomes when they induce fragmentation on either side of the nucleosomes (*67*). Fragments between 180 and 247 base pairs (bp) can be assumed to represent mononucleosomes based on their size (*67*). Therefore, removal of 180- to 247-bp sequence fragments from the

analysis can reveal the position of mononucleosomes near TSSs (*67*). To determine the extent to which Zld-bound sites near TSSs coincided with mononucleosomes, we examined the ATAC-seq data from regenerating discs in which 180- to 247-bp fragments had been bioinformatically removed (nucleosome-free) and compared it to data that included those sequences (nucleosome) (Fig. 8L) (*64*). Many Zld-bound TSSs, such as those at the two alternative TSSs for *ct*, showed evidence of single nucleosomes during regeneration (Fig. 8L). These regions had one broad peak in the "nucleosome" dataset and two peaks flanking a space in the "nucleosome-free" dataset, suggesting the presence of mononucleosomes at the TSSs. Thus, Zld may bind mononucleosomes that regulate access to promoter regions near key developmental genes, as it facilitates the exit from regeneration and the return to normal patterning.

DISCUSSION

Here, we have shown that the pioneer transcription factor Zld controls the timing and extent of cell fate, patterning, and integrin gene expression, as the regenerating wing disc transitions to normal development during late regeneration. Regeneration has long been thought to deploy developmental mechanisms to repair and regrow the tissue (*68*, *69*), a notion that has been challenged recently. For example, in amniote limb regeneration, *fgf10*, a gene important for normal limb development, is not important for limb regeneration (*70*). Conversely, during *Xenopus* limb regeneration, the homeotic transcription factors Homeobox 12 (Hox12) and Hoxc13 promote expression of developmental genes, while being dispensable for limb development (*71*). Similarly, the genes *tara* and *brat* are required for cell fate preservation in regenerating *Drosophila* wing imaginal discs but not in normally developing discs (*36*, *38*). The involvement of pioneer factors in late regeneration events, including the exit from the damage response and restoration of developmental patterning, is an important paradigm for how regeneration is orchestrated. Single-cell sequencing analysis of regenerating imaginal discs has led to the proposal that the regenerating tissue resembles an early developmental stage (*72*). Perhaps, Zld facilitates the transition from this younger state to an age-appropriate state. We propose that regeneration does not cease simply because damage-response signaling comes to an end or the tissue reaches a critical size but instead ceases through an active mechanism that restores expression of developmental genes, coordinated by pioneer factors.

Pioneer transcription factors play a crucial role in facilitating cell fate reprogramming across diverse developmental contexts. For instance, Gata4 induces the conversion of fibroblasts to cardiomyocyte-like cells, Achaete-Scute Family BHLH Transcription Factor 1 (Ascl1) promotes the differentiation of glutamatergic neurons from fibroblasts, and FoxA facilitates the reprogramming of cells into hepatocyte-like states from fibroblasts (*73*). These findings emphasize the relationship between pioneer factors and diversification of cell fate from undifferentiated precursors. In regenerating wing imaginal discs, pioneer factors may have a similar role in reactivation of cell fates from despecified cell populations, such as the regeneration blastema.

While Zld was identified as a pioneering transcription factor in the *Drosophila* embryo, where it often binds CAGGTAG sites (*9*), Zld binding of these embryonic CAGGTAG sites is not as enriched in the neuroblast (*17*), nor are most of these sites bound by Zld in the regenerating wing disc (Fig. 3C). In addition, most of the sites that were bound in the neuroblast and the regenerating wing disc did not have the CAGGTAG motif. Recent analysis has identified embryonic Zld binding to low-affinity motifs that deviate slightly from the canonical motif (*65*), and a search for those motifs in the Zld-bound regions in the wing disc found very few, leaving much of Zld's binding in the wing disc unexplained. However, expression of Zld in *Drosophila* S2 cells, where it is not normally expressed, identified many regions where Zld bound and caused changes in chromatin accessibility. Only 45% of these regions contained an embryonic Zld motif, indicating that most of the regions where Zld acted as a pioneer factor bound Zld in some other way (*74*).

There is also little overlap between Zld binding sites in the neuroblast and the regenerating wing disc, nor are there common motifs found at the bound sites, except for the GAF motif. Perhaps, the tissue-specific binding of Zld is directed by transcription factors that bind the motifs enriched in the Zld-binding sites in each tissue. Of these, the Fkh binding motif and the CA-rich repeats were the most prominent in the regenerating disc (Fig. 8A), although others were present (fig. S8A). The similar phenotypes when GAF and Fkh levels were reduced during regeneration support our model that they act at the same loci as Zld. Prior work comparing Zld binding in different cell types, including S2 cells that do not normally express Zld, suggests that Zld binding is influenced by the activity of tissue-specific transcription factors (*74*).

Work in the embryo using loss-of-function analysis (*15*) and deep learning using genomic data (*65*) suggests that chromatin at some Zld-bound sites remains open in the absence of Zld and that expression of patterning genes is still activated but with delayed timing. Our finding that the transition from regeneration gene expression to normal patterning is delayed when Zld is inactivated and that the eventual repatterning is aberrant is consistent with these models. Thus, Zld may similarly act as a potentiator of patterning gene expression during the exit from regeneration.

One open question is why Zld is present according to our immunostaining in undamaged discs but does not appear to bind near genes to any appreciable extent and has no effect when depleted? One possible clue comes from work in which Zld was expressed at varying concentrations in both S2 cells and neuroblasts, which showed that higher expression induced binding at substantially more loci and increased changes in chromatin accessibility (*74*). Thus, the increase in expression between undamaged and regenerating tissue may cross some threshold needed for consistent Zld binding. Furthermore, Zld interacts with DNA in subregions of the nucleus called "hubs" (*75*). Perhaps, Zld in the undamaged wing disc is not recruited to these hubs or is actively sequestered from these hubs, or these hubs do not form until a minimum threshold level of Zld occurs. Alternatively, there may be transcription factors present in the regenerating tissue that are not normally present in an undamaged disc that facilitate Zld binding.

In addition to regulating target genes directly, we established that Zld can influence cell fate through Notch signaling, as we confirmed that the Notch ligand *Dl* is a target of Zld (Fig. 4N and fig. S4, J to M). We also found Zld bound near additional Notch signaling pathway components and regulators, including *E(spl)Mβ*, *serrate*, *Notch*, and *mastermind*. Thus, Zld could be regulating Notch signaling in general, exacerbating some of the Zld phenotypes related to *ct* and *ac*, as these genes are downstream of Notch (*76*, *77*) and direct targets of Zld.

The damage in this study was induced by ablation of a large area of tissue, which took place over some time. It is possible that the

method of damage in imaginal discs has some effect on the regulation of subsequent regeneration. However, the same mechanisms of regeneration have been observed after both tissue ablation and mechanical disruption, including JNK signaling (*78*–*80*), Wg and Myc expression (*8*), and loss of patterning gene expression (*7*, *8*), and many, although not all, of the same regeneration genes are upregulated (*81*–*83*). Thus, this understanding of the role of pioneer transcription factors may be broadly applicable to regeneration regardless of the mode of tissue damage.

Several pioneer factors are important for the initial response to tissue damage in a variety of damage models. For example, a recent report suggested that Zld is important for appendage regrowth in the American cockroach (*84*), establishing Zld as a regeneration factor in a different insect and a different role in regeneration. In another invertebrate, the acoel worm, the *egr* acts as a pioneer factor to regulate early wound genes (*85*). In vertebrates, the pioneer factors Sox2 and Klf4 are required for reprogramming retinal cells during retinal ganglion cell regeneration (*42*). Thus, pioneer transcription factors such as Zld, Egr, Sox2, and Klf may play distinct roles in a variety of transitions such as the initial damage response (acoel worm, vertebrate retinal cells), tissue regrowth between exoskeleton molts (cockroach), and restoration of pattern and cell fate to form a functional organ or limb (*Drosophila*). The work presented here establishes the role of these factors in late regeneration and the return to normal gene expression. Future work may uncover pioneer factors playing similar roles in regeneration across species and may be deployed to control the exit from regeneration in therapeutic models.

MATERIALS AND METHODS

Tissue ablation

Ablation and regeneration studies were carried out as previously described (*8*). Briefly, egg lays were carried out at room temperature in the dark for 4 hours on grape juice plates with yeast paste, after which they were kept at 18°C. Approximately 50 hatched larvae were collected in separate Nutri-Fly Bloomington food (Genessee Scientific, 66-112) vials with yeast paste added and food churned. At early day 7, when larvae are at early third instar stage as determined by mouth hooks, damage was induced by *reaper* by placing the vials in a circulating water bath at 30°C for 24 hours. The vials were then cooled in an ice water bath for 60 s and returned to an 18°C incubator. The regenerating animals were either dissected according to the required time point or allowed to develop to adulthood to assess adult wing size and patterning. Undamaged animals were kept consistently at 18°C and were dissected on day 10 after egg laying, just before pupariation. For the regeneration experiments driving *rpr* expression using *salm-GAL4*, the protocol outlined in (*11*) was followed, with tissue ablation occurring over a 16-hour period.

Fly stocks

The fly stocks used for this study were as follows: w^{1118} [Bloomington Drosophila Stock Center (BDSC), #3605], y1 w^{*}; P{rn-GFP.FPTB} attP40 (BDSC, #93091), w^{1118};;UAS-rpr,rnGAL4,Gal80^{ts}/TM6B,Gal80 (*8*), y1 w^{*}; PBac{bs-GFP.FPTB}VK00031 (BDSC, #93568), w^{*}; l(2)**/CyO, P{en1}wgen11; P{E(spl)mβ-HLH-CD2.dC}T6 (BDSC, #83353), CRY2::ZLD (gift from M. Harrison) (*11*), w1118; P{GMR11F02-lexA} JK22C (BDSC, #94749), y1 w^{*}; PBac{13XLexAop2-mCherry-Rab3} VK00018/CyO, P{Wee-P.ph0}BaccWee-P20; Dr^{1}/TM6C, Sb^{1} Tb^{1} (BDSC, #52252), y^{1} w^{67c23};+; P{CaryP}attP2 (BDSC, #8622), w^{67c23};13xLexAop–short hairpin RNA (shRNA)–zld;+ (this study), w^{67c23};+;13xLexAop-shRNA-zld (this study), tara$^{UAS.Tag:MYC}$ (*86*), w^{*}; P{neoFRT}82B osa^{308}/TM6B, Tb^{1} (BDSC, #5949), w1118; tara1/TM3, Sb (BDSC, #6403), P{PZ}tara03881 ry^{506}/TM3, ry^{RK} Sb^{1} Ser^{1} (BDSC, #11613), w[1]; Trl[13C]/TM6B, Sb[1] Tb[1] (BDSC, #58473), y[1] v[1]; P{y[+t7.7] v[+t1.8] = TRiP.JF02417}attP2 (BDSC, #27072), y[1] sc[*] v[1] sev[21]; P{y[+t7.7] v[+t1.8] = TRiP.HMS01103}attP2 (BDSC, #33760), y[1] v[1]; P{y[+t7.7] = CaryP}attP2 (BDSC, #36303), w[*]; P{y[+t7.7] w[+mC] = lexAop-rCD2.RFP.lexAop-GFPi}attP2 (BDSC, #56175), +;+;GAF::GFP (gift from M. Harrison) (*16*), +;+;UASt-Zld (gift from M. Harrison) (*17*), GFP::Zld;+;+ (gift from M. Harrison) (*43*), and w*;P{arm-GFP.P}83 (BDSC, #8555).

Optogenetic inactivation of Zld

Optogenetic inactivation experiments were carried out by placing food vials containing undamaged or damaged larvae about 3 inches (7.62 cm) away from blue LED lights (KQHBEN) inside an 18°C incubator, thus ensuring that temperature was controlled. Blue light exposure occurred between the 8th and 11th days after egg lay for both damaged and undamaged animals homozygous for *CRY2::zld* that had spent 24 hours in the 30°C water bath. For experiments in which Zld was inactivated in flies containing Bs-GFP and UAS-tara, only males hemizygous for *CRY2::zld* were dissected and/or analyzed. Undamaged animals for these experiments were exposed to equal amount of blue light but kept at 18°C throughout. For control experiments, *CRY2::zld* flies were continuously kept in the dark to ensure no Zld inactivation caused by normal bright light.

Immunofluorescence

Immunostaining was carried out as previously described (*8*). Primary antibodies were used at the following concentrations: anti-Zld (1:1000) (gift from M. Harrison) (*87*), anti-Nubbin (1:100) [Developmental Studies Hybridoma Band (DSHB), 2D4), anti-Ct (1:150) (DSHB, 2b10), anti-CD2 (1:500) (Bio-Rad, catalog no. MCA154R), anti-Dl (1:400) (DSHB, c594.9b), anti-Wg (1:100) (DSHB, 4D4), anti-Frizzled2 (1:50) (DSHB, 1A3G4), anti-Ac (1:10) (DSHB, RRID AB_528066), anti-Ptc (1:50) (DSHB, Apa1), anti-En (1:3) (DSHB, 4D9), anti-Osa (1:1) (DSHB, RRID AB_528420), anti–β-galactosidase (1:500) (Thermo Fisher Scientific, catalog no. A-11132), anti-Mys (1:50) (DSHB, cf.6 g11), anti-Mew (1:50) (DSHB, DK.1A4), anti–phospho–Histone H3 (1:500) (DSHB, 06-570), anti-GFP (1:500) (Abcam, Ab290), anti-GFP (1:1000) (Invitrogen, 3E6), and anti-Arm (1:50) (DSHB, N2 7A1). Secondary antibodies used were Alexa Fluor 555 goat anti-mouse immunoglobulin G (IgG) (1:1000) (Invitrogen, catalog no. A21424), Alexa Fluor 555 goat anti-rabbit IgG (1:1000) (Invitrogen, A21429), Alexa Fluor 488 goat anti-rabbit IgG (1:1000) (Invitrogen, A11034), and Alexa Fluor 488 goat anti-mouse IgG (1:1000) (Invitrogen, A11001). The nuclear stain 4′,6-diamidino-2-phenylindole was used at a 1:1000 dilution (Thermo Fisher Scientific, D1306). Normal goat serum (NGS; 5%) was used as a blocking agent (Thermo Fisher Scientific, 31872). Immunostained samples were mounted on VECTASHIELD antifade mounting medium (Vector Laboratories, H-1000).

All immunofluorescence images were captured using a Zeiss LSM700 or LSM900 confocal microscope. The same microscope and settings were used for all images in a given experiment. Maximum intensity projections were used for quantifying protein expression pattern or intensity in the regenerating pouch, which was demarcated by Nubbin expression or by generating a 150 pixel–by–150 pixel area in the center of the pouch area. Images were processed and quantified

using FIJI, and parameters and settings for quantified images were kept the same for all images in a given experiment. Percentage of D/V boundary expressing Ct was calculated using the freehand line tool in FIJI to draw a line across Ct expression along the D/V boundary and measuring length of expression divided by full D/V boundary length. Area of En silencing in the posterior compartment was calculated by outlining the area where En was repressed using the freehand selection tool in FIJI. The same method was used for calculating the ectopic Ptc expression in the posterior compartment.

Adult wing quantification

Adult wings were mounted with Canada balsam (MilliporeSigma, C1795-25ml) dissolved in methyl salicylate (Acros Organics, catalog no. 220495000). Images were taken on an Echo Revolve R4 microscope and were processed using FIJI. Percentage of veins present was calculated using the freehand line tool in FIJI to measure actual vein length divided by presumptive full vein length.

Quantitative polymerase chain reaction

qPCR experiments were carried out as described previously (*36*). Briefly, 20 to 30 discs were collected in Schneiders insect medium (Sigma-Aldrich, S1046-500ml), and the total RNA was extracted using the RNeasy Mini Kit (QIAGEN, 74104). Approximately 100 ng of RNA was used for each sample to make cDNA using the SuperScript III First Strand Synthesis Kit (Thermo Fisher Scientific, 11752-050). The qPCR reaction was made with addition of SYBR Green Master Mix (Thermo Fisher Scientific, A25742) and then run on an ABI StepOnePlus Real-Time PCR System. Each experiment included three biological replicates, with three technical replicates each. Fold changes were then calculated according to the $\Delta\Delta C_t$ method, using glyceraldehyde-3-phosphate dehydrogenase 2 (GAPDH2) as a comparative housekeeping gene. The primers used for Zld and GAPDH2 quantification can be found in table S1.

CUT&RUN experiment

For the CUT&RUN experiments, we used flies homozygous for a functional, endogenous Zld tagged with superfolder GFP (*43*) together with an anti-GFP antibody (Abcam, Ab290).We used *zldGFP;+;UAS-rpr,rnGAL4,Gal80^{ts}*/+ flies for regenerating discs and *zldGFP;+;+* for undamaged flies. Control experiments also used *w^{1118};+;UAS-rpr,rnGAL4,Gal80^{ts}*/+ discs that lacked GFP-tagged Zld. Two replicates were performed for each genotype and condition. All reagents used were from the CUT&RUN assay kit (Cell Signaling Technology, 86652). For each replicate, 100 wing discs were dissected from R48 or undamaged larvae into 1× wash buffer (350 µl of 10× wash buffer, 35 µl of 100× spermidine, 17.5 µl of 200× protease inhibitor cocktail, and 3097.5 µl of nuclease-free water). Discs were then suspended in activated concanavalin A beads, after which antibody binding buffer (1 µl of 100× spermidine, 0.5 µl of 200× protease inhibitor cocktail, 2.5 µl of digitonin solution, 0.2 µl of GFP antibody, and 95.8 µl of antibody buffer) was added to the sample for primary antibody binding and kept on a nutator overnight in 4°C. Next, the samples were treated with 1.5 µl of pAG-MNase (Protein A/Protein G fused to Micrococcal Nuclease) enzyme in 50 µl of digitonin buffer (4.56 µl of 10× wash buffer, 0.46 µl of 100× spermidine, 0.23 µl of 200× protease inhibitor cocktail, 1.14 µl of digitonin solution, and 40.6 µl of nuclease-free water), followed by incubation at 4°C for 1 hour. DNA digestion was performed by activating the pAG-MNase enzyme with 3 µl of $CaCl_2$ for 30 min at 4°C. The reaction was stopped, and chromatin was released by adding the sample with 150 µl of 1× stop buffer, which included the spike-in yeast DNA (37.5 µl of 4× stop buffer, 3.75 µl of digitonin solution, 0.75 µl of ribonuclease A, 5 µl of yeast spike-in, and 103 µl of nuclease-free water), incubating at 37°C for 15 min. The released chromatin was then purified using the DNA purification buffer and spin columns kit (Cell Signaling Technology, 14209S). The libraries were prepared by the Roy J. Carver Biotechnology Center, DNA Services facility using the Ultralow Input Library construction kit from Tecan. Samples were sequenced in the DNA Services facility on a NovaSeq 6000 (101 cycles) from both ends using V1.5 sequencing kits. Fastq files were generated and demultiplexed with the bcl2fastq v2.20 conversion software (Illumina).

CUT&RUN data processing

The CUT&RUN paired-end reads were aligned to the *Drosophila melanogaster* dm6 genome (Release 6 plus ISO1 MT, version 2014) and *Saccharomyces cerevisiae* genome version R64 using bowtie2 (*88*). Alignment parameters included --very-sensitive-local --no unal –no-mixed --no-discordant --phred33 -I 10 -X 700 –local--no-overlap --no dovetail. Reads were then sorted according to coordinates using SAMtools (*89*). The resultant files were processed with MarkDuplicates (Broad Institute) for identifying and removing PCR duplicates with high stringency. The coverage file was normalized and scaled in accordance to reads aligned to the spike-in (*S. cerevsiae*) using genomcov, part of bedtools. The continuous coverage file was obtained using bamCoverage, part of deepTools (*48*), which was normalized either to spike-in DNA or to 1× depth (reads per genome coverage). Data range for coverage files in each figure was set between 0 and 10 except for *ac* (0 to 4.5), *tara* (0 to 15), and *osa* (0 to 15). Peak calling was done using MACS2 (*47*) with default parameters. Tracks were visualized using Integrative Genomics Viewer (IGV). Peak files were annotated using ChIPseeker (*46*), and a heatmap was made using plotHeatmap, part of deepTools (*48*). Peak-called files were converted to FASTA sequence using Extract Genomic DNA tool, part of Galaxy tools. Motif discovery and analysis were carried out using peak-called FASTA files in MEME-ChIP in discriminative mode, part of MEME Suite (*90*). To examine GAF and Fkh motif annotation within Zld peaks, their enriched motif GFF3 files from MEME-ChIP analysis for Zld at R48 were downloaded and converted to BED files, which were then used as the input for the ChIPseeker tool. Generated CUT&RUN data were compared to ChIP-seq data for Zld in stage 14 embryo (GSE 30757) and type II neuroblast (GSE 150931). To scan for CAGGTA and TAGGTAG motifs, we used FIMO motif scanning tool (*91*) with a threshold of 1×10^{-4} *P* value.

LexAop-shRNA-*zld* generation

To make a stable *Drosophila* line with RNAi-mediated knockdown of *zld*, the passenger strand previously described (*15*), specific to the *zld* transcript, was cloned into a LexAop-pWALIUM20 vector using services from GenScript (table S1). The hairpin sequence used was TAGTTATATTCAAGCATA. The plasmid was then injected into embryos and integrated into the *Drosophila* genome at the attP40 and attP2 recombination sites using services from BestGene.

ATAC-seq data analysis

Processed files from Gene Expression Omnibus (GEO) accession ID GSE102841 (*64*) were used to analyze chromatin accessibility at

Zld-bound regions in early (R0) and mid (R15) regeneration in *Drosophila* wing imaginal discs. The coverage files for the control undamaged discs were subtracted from the coverage files for the regenerating discs, followed by combining the resultant files for each replicate. Final tracks were compared between R0 and R15 time points while keeping the data ranges the same. Tracks were viewed on IGV.

Proximity Ligation Assay

The Proximity Ligation Assay was performed using the Duolink In Situ Mouse/Rabbit Detection Kits (#DUO92008) following the manufacturer's instructions, with minor modifications. Larvae were dissected at the desired time point in phosphate-buffered saline (PBS), and the posterior half was removed. The remaining half was inverted using forceps to expose the wing imaginal discs. Larval carcasses were fixed in 4% paraformaldehyde for 20 min at room temperature, followed by three washes with 0.1% PBST (PBS + 0.1% Triton X-100), each lasting 10 min. Primary antibodies were diluted to the appropriate concentrations in a solution containing 5% NGS and PBST, and the samples were incubated overnight at 4°C. After three washes in PBST, individual carcasses were transferred to 0.5-ml tubes. The Duolink PLA plus and minus probes (#DUO92101) were diluted 1:5 in the supplied antibody diluent, and 20 µl of the probe mix was added to each tube. Samples were incubated overnight at 4°C to allow probe binding and proximity ligation. The following day, the probe mix was removed, and the samples were washed three times in PBST, with each wash lasting 10 min. For the ligation step, 5× Duolink Ligation Buffer was diluted 1:5 with molecular-grade water (Corning, 46-000-CM) to prepare a 19.5 µl of reaction mix per sample. Immediately before use, 0.5 µl of ligase was added to the reaction mix (1:40), and 20 µl of the final solution was added to each sample. The samples were incubated for 2 hours at 37°C in a water bath. After the ligation step, the solution was removed, and each sample went through 3× 10-min washes in PBST. For the amplification step, 5× amplification buffer, which contains the detection oligos coupled to fluorochromes, was diluted 1:5 in molecular-grade water to prepare 19.75 µl of reaction mix per sample. Immediately before use, 0.25 µl of polymerase (1:80) was added to each mix, and 20 µl of the final solution was applied to each sample. Samples were incubated for 2 hours at 37°C in a water bath. After amplification, the reaction solution was removed, and the samples were washed twice for 10 min each in 1× wash buffer B (#DUO82049), followed by a final wash in 0.01× wash buffer B for 1 min. The wing discs were mounted on slides using VECTASHIELD mounting medium and secured with coverslips for imaging.

PLA focus counting

To quantify PLA signal, a 100 pixel–by–60 pixel box was made in the wing pouch area of discs, and the foci were counted using the multipoint tool in ImageJ.

Statistical analysis

For measuring relevant statistical differences of means between two groups, the two-tailed Student's *t* test method was applied. For comparing multiple groups, the one-way analysis of variance (ANOVA) statistical test was applied. For comparing wing sizes between different groups, a chi-square test was performed. Analysis and graphs were made using GraphPad Prism 10.

Supplementary Materials

The PDF file includes:
Figs. S1 to S10
Table S1
Legends for tables S2 and S3

Other Supplementary Material for this manuscript includes the following:
Tables S2 and S3

REFERENCES AND NOTES

1. K. D. Poss, L. G. Wilson, M. T. Keating, Heart regeneration in Zebrafish. *Science* **298**, 2188–2190 (2002).
2. M. H. Yun, H. Davaapil, J. P. Brockes, Recurrent turnover of senescent cells during regeneration of a complex structure. *eLife* **4**, e05505 (2015).
3. M. H. Mokalled, K. D. Poss, A regeneration toolkit. *Dev. Cell* **47**, 267–280 (2018).
4. S. Rafii, J. M. Butler, B.-S. Ding, Angiocrine functions of organ-specific endothelial cells. *Nature* **529**, 316–325 (2016).
5. J. M. Wells, F. M. Watt, Diverse mechanisms for endogenous regeneration and repair in mammalian organs. *Nature* **557**, 322–328 (2018).
6. I. K. Hariharan, F. Serras, Imaginal disc regeneration takes flight. *Curr. Opin. Cell Biol.* **48**, 10–16 (2017).
7. S. Díaz-García, A. Baonza, Pattern reorganization occurs independently of cell division during *Drosophila* wing disc regeneration in situ. *Proc. Natl. Acad. Sci. U.S.A.* **110**, 13032–13037 (2013).
8. R. K. Smith-Bolton, M. I. Worley, H. Kanda, I. K. Hariharan, Regenerative growth in *Drosophila* imaginal discs is regulated by Wingless and Myc. *Dev. Cell* **16**, 797–809 (2009).
9. M. M. Harrison, X.-Y. Li, T. Kaplan, M. R. Botchan, M. B. Eisen, Zelda binding in the early *Drosophila melanogaster* embryo marks regions subsequently activated at the maternal-to-zygotic transition. *PLOS Genet.* **7**, e1002266 (2011).
10. H.-L. Liang, C.-Y. Nien, H.-Y. Liu, M. M. Metzstein, N. Kirov, C. Rushlow, The zinc-finger protein Zelda is a key activator of the early zygotic genome in *Drosophila*. *Nature* **456**, 400–403 (2008).
11. S. L. McDaniel, T. J. Gibson, K. N. Schulz, M. F. Garcia, M. Nevil, S. U. Jain, P. W. Lewis, K. S. Zaret, M. M. Harrison, Continued activity of the pioneer factor Zelda is required to drive zygotic genome activation. *Mol. Cell* **74**, 185–195.e4 (2019).
12. C.-Y. Nien, H.-L. Liang, S. Butcher, Y. Sun, S. Fu, T. Gocha, N. Kirov, J. R. Manak, C. Rushlow, Temporal coordination of gene networks by Zelda in the early *Drosophila* embryo. *PLOS Genet.* **7**, e1002339 (2011).
13. K. N. Schulz, E. R. Bondra, A. Moshe, J. E. Villalta, J. D. Lieb, T. Kaplan, D. J. McKay, M. M. Harrison, Zelda is differentially required for chromatin accessibility, transcription factor binding, and gene expression in the early *Drosophila* embryo. *Genome Res.* **25**, 1715–1726 (2015).
14. N. Staudt, S. Fellert, H.-R. Chung, H. Jäckle, G. Vorbrüggen, Mutations of the *Drosophila* zinc finger-encoding gene *vielfältig* impair mitotic cell divisions and cause improper chromosome segregation. *Mol. Biol. Cell* **17**, 2356–2365 (2006).
15. Y. Sun, C.-Y. Nien, K. Chen, H.-Y. Liu, J. Johnston, J. Zeitlinger, C. Rushlow, Zelda overcomes the high intrinsic nucleosome barrier at enhancers during *Drosophila* zygotic genome activation. *Genome Res.* **25**, 1703–1714 (2015).
16. M. M. Gaskill, T. J. Gibson, E. D. Larson, M. M. Harrison, GAF is essential for zygotic genome activation and chromatin accessibility in the early *Drosophila* embryo. *eLife* **10**, e66668 (2021).
17. E. D. Larson, H. Komori, T. J. Gibson, C. M. Ostgaard, D. C. Hamm, J. M. Schnell, C.-Y. Lee, M. M. Harrison, Cell-type-specific chromatin occupancy by the pioneer factor Zelda drives key developmental transitions in *Drosophila*. *Nat. Commun.* **12**, 7153 (2021).
18. M. L. Golson, K. H. Kaestner, Fox transcription factors: From development to disease. *Development* **143**, 4558–4570 (2016).
19. J. Judd, F. M. Duarte, J. T. Lis, Pioneer-like factor GAF cooperates with PBAP (SWI/SNF) and NURF (ISWI) to regulate transcription. *Genes Dev.* **35**, 147–156 (2021).
20. A. R. Brock, M. Seto, R. K. Smith-Bolton, Cap-n-Collar promotes tissue regeneration by regulating ROS and JNK signaling in the *Drosophila melanogaster* wing imaginal disc. *Genetics* **206**, 1505–1520 (2017).
21. S. E. St Pierre, M. I. Galindo, J. P. Couso, S. Thor, Control of *Drosophila* imaginal disc development by rotund and roughened eye: Differentially expressed transcripts of the same gene encoding functionally distinct zinc finger proteins. *Development* **129**, 1273–1281 (2002).
22. S. E. McGuire, Z. Mao, R. L. Davis, Spatiotemporal gene expression targeting with the TARGET and gene-switch systems in *Drosophila*. *Sci. STKE* **2004**, pl6-pl6 (2004).
23. A. C. Aplin, T. C. Kaufman, Homeotic transformation of legs to mouthparts by proboscipedia expression in *Drosophila* imaginal discs. *Mech. Dev.* **62**, 51–60 (1997).

24. A. Repiso, C. Bergantiños, F. Serras, Cell fate respecification and cell division orientation drive intercalary regeneration in *Drosophila* wing discs. *Development* **140**, 3541–3551 (2013).
25. J. Jack, D. Dorsett, Y. Delotto, S. Liu, Expression of the cut locus in the *Drosophila* wing margin is required for cell type specification and is regulated by a distant enhancer. *Development* **113**, 735–747 (1991).
26. J. J. Krupp, L. E. Yaich, R. J. Wessells, R. Bodmer, Identification of genetic loci that interact with cut during *Drosophila* wing-margin development. *Genetics* **170**, 1775–1795 (2005).
27. U. Nussbaumer, G. Halder, J. Groppe, M. Affolter, J. Montagne, Expression of the blistered/DSRF gene is controlled by different morphogens during *Drosophila* trachea and wing development. *Mech. Dev.* **96**, 27–36 (2000).
28. F. Roch, A. Baonza, E. Martín-Blanco, A. García-Bellido, Genetic interactions and cell behaviour in blistered mutants during proliferation and differentiation of the *Drosophila* wing. *Development* **125**, 1823–1832 (1998).
29. J. F. de Celis, A. Garcia-Bellido, S. J. Bray, Activation and function of Notch at the dorsal-ventral boundary of the wing imaginal disc. *Development* **122**, 339–369 (1996).
30. V. M. Panin, V. Papayannopoulos, R. Wilson, K. D. Irvine, Fringe modulates Notch–ligand interactions. *Nature* **387**, 908–912 (1997).
31. D. Doherty, G. Feger, S. Younger-Shepherd, L. Y. Jan, Y. N. Jan, Delta is a ventral to dorsal signal complementary to Serrate, another Notch ligand, in *Drosophila* wing formation. *Genes Dev.* **10**, 421–434 (1996).
32. N. E. Baker, Transcription of the segment-polarity gene wingless in the imaginal discs of *Drosophila*, and the phenotype of a pupal-lethal *wg* mutation. *Development* **102**, 489–497 (1988).
33. M. Rosales-Vega, D. Reséndez-Pérez, M. Zurita, M. Vázquez, TnaA, a trithorax group protein, modulates wingless expression in different regions of the *Drosophila* wing imaginal disc. *Sci. Rep.* **13**, 15162 (2023).
34. J. A. Williams, S. W. Paddock, S. B. Carroll, Pattern formation in a secondary field: A hierarchy of regulatory genes subdivides the developing *Drosophila* wing disc into discrete subregions. *Development* **117**, 571–584 (1993).
35. D. del Alamo Rodríguez, J. Terriente, M. I. Galindo, J. P. Couso, F. J. Díaz-Benjumea, Different mechanisms initiate and maintain wingless expression in the *Drosophila* wing hinge. *Development* **129**, 3995–4004 (2002).
36. S. N. F. Abidi, F. T.-Y. Hsu, R. K. Smith-Bolton, Regenerative growth is constrained by brain tumor to ensure proper patterning in *Drosophila*. *PLOS Genet.* **19**, e1011103 (2023).
37. Y. Tian, R. K. Smith-Bolton, Regulation of growth and cell fate during tissue regeneration by the two SWI/SNF chromatin-remodeling complexes of *Drosophila*. *Genetics* **217**, 1–16 (2021).
38. K. J. Schuster, R. K. Smith-Bolton, Taranis protects regenerating tissue from fate changes induced by the wound response in *Drosophila*. *Dev. Cell* **34**, 119–128 (2015).
39. M. Iwafuchi-Doi, K. S. Zaret, Pioneer transcription factors in cell reprogramming. *Genes Dev.* **28**, 2679–2692 (2014).
40. T. Katsuda, J. H. Sussman, K. Ito, A. Katznelson, S. Yuan, N. Takenaka, J. Li, A. J. Merrell, H. Cure, Q. Li, R. U. Rasool, I. A. Asangani, K. S. Zaret, B. Z. Stanger, Cellular reprogramming in vivo initiated by SOX4 pioneer factor activity. *Nat. Commun.* **15**, 1761 (2024).
41. Y. Yang, N. Gomez, N. Infarinato, R. C. Adam, M. Sribour, I. Baek, M. Laurin, E. Fuchs, The pioneer factor SOX9 competes for epigenetic factors to switch stem cell fates. *Nat. Cell Biol.* **25**, 1185–1195 (2023).
42. Y. Lu, B. Brommer, X. Tian, A. Krishnan, M. Meer, C. Wang, D. L. Vera, Q. Zeng, D. Yu, M. S. Bonkowski, J.-H. Yang, S. Zhou, E. M. Hoffmann, M. M. Karg, M. B. Schultz, A. E. Kane, N. Davidsohn, E. Korobkina, K. Chwalek, L. A. Rajman, G. M. Church, K. Hochedlinger, V. N. Gladyshev, S. Horvath, M. E. Levine, M. S. Gregory-Ksander, B. R. Ksander, Z. He, D. A. Sinclair, Reprogramming to recover youthful epigenetic information and restore vision. *Nature* **588**, 124–129 (2020).
43. D. C. Hamm, E. D. Larson, M. Nevil, K. E. Marshall, E. R. Bondra, M. M. Harrison, A conserved maternal-specific repressive domain in Zelda revealed by Cas9-mediated mutagenesis in *Drosophila melanogaster*. *PLOS Genet.* **13**, e1007120 (2017).
44. K. R. Chang, D. D. Tsao, C. Bennett, E. Wang, J. F. Floyd, A. S. Y. Tay, E. Greenwald, E. S. Kim, C. Griffin, E. Morse, T. Chisholm, A. E. Rankin, L. A. Baena-Lopez, N. Lantz, E. Fox, L. Kockel, S. K. Kim, S. Park, Transgenic *Drosophila* lines for LexA-dependent gene and growth regulation. *G3 (Bethesda)* **12**, jkac018 (2022).
45. P. J. Skene, S. Henikoff, An efficient targeted nuclease strategy for high-resolution mapping of DNA binding sites. *eLife* **6**, e21856 (2017).
46. G. Yu, L.-G. Wang, Q.-Y. He, ChIPseeker: An R/Bioconductor package for ChIP peak annotation, comparison and visualization. *Bioinformatics* **31**, 2382–2383 (2015).
47. Y. Zhang, T. Liu, C. A. Meyer, J. Eeckhoute, D. S. Johnson, B. E. Bernstein, C. Nusbaum, R. M. Myers, M. Brown, W. Li, X. S. Liu, Model-based analysis of ChIP-seq (MACS). *Genome Biol.* **9**, R137 (2008).
48. F. Ramírez, D. P. Ryan, B. Grüning, V. Bhardwaj, F. Kilpert, A. S. Richter, S. Heyne, F. Dündar, T. Manke, deepTools2: A next generation web server for deep-sequencing data analysis. *Nucleic Acids Res.* **44**, W160–W165 (2016).
49. V. Chaudhary, S. Hingole, J. Frei, F. Port, D. Strutt, M. Boutros, Robust Wnt signaling is maintained by a Wg protein gradient and Fz2 receptor activity in the developing *Drosophila* wing. *Development* **146**, dev174789 (2019).
50. C. A. Micchelli, E. J. Rulifson, S. S. Blair, The function and regulation of cut expression on the wing margin of *Drosophila*: Notch, Wingless and a dominant negative role for Delta and Serrate. *Development* **124**, 1485–1495 (1997).
51. S. S. Huppert, T. L. Jacobsen, M. A. T. Muskavitch, Feedback regulation is central to Delta-Notch signalling required for *Drosophila* wing vein morphogenesis. *Development* **124**, 3283–3291 (1997).
52. J. P. Couso, S. A. Bishop, A. M. Arias, The wingless signalling pathway and the patterning of the wing margin in *Drosophila*. *Development* **120**, 621–636 (1994).
53. F. J. Diaz-Benjumea, S. M. Cohen, Serrate signals through Notch to establish a Wingless-dependent organizer at the dorsal/ventral compartment boundary of the *Drosophila* wing. *Development* **121**, 4215–4225 (1995).
54. E. Gracia-Latorre, L. Pérez, M. Muzzopappa, M. Milán, A single WNT enhancer drives specification and regeneration of the *Drosophila* wing. *Nat. Commun.* **13**, 4794 (2022).
55. R. E. Harris, L. Setiawan, J. Saul, I. K. Hariharan, Localized epigenetic silencing of a damage-activated WNT enhancer limits regeneration in mature *Drosophila* imaginal discs. *eLife* **5**, e11588 (2016).
56. D. L. Brower, M. Wilcox, M. Piovant, R. J. Smith, L. A. Reger, Related cell-surface antigens expressed with positional specificity in *Drosophila* imaginal discs. *Proc. Natl. Acad. Sci. U.S.A.* **81**, 7485–7489 (1984).
57. M. C. Diaz de la Loza, B. J. Thompson, Forces shaping the *Drosophila* wing. *Mech. Dev.* **144**, 23–32 (2017).
58. D. Fristrom, M. Wilcox, J. Fristrom, The distribution of PS integrins, laminin A and F-actin during key stages in *Drosophila* wing development. *Development* **117**, 509–523 (1993).
59. O. Söderberg, M. Gullberg, M. Jarvius, K. Ridderstråle, K.-J. Leuchowius, J. Jarvius, K. Wester, P. Hydbring, F. Bahram, L.-G. Larsson, U. Landegren, Direct observation of individual endogenous protein complexes in situ by proximity ligation. *Nat. Methods* **3**, 995–1000 (2006).
60. R. A. Cavallo, R. T. Cox, M. M. Moline, J. Roose, G. A. Polevoy, H. Clevers, M. Peifer, A. Bejsovec, *Drosophila* Tcf and Groucho interact to repress Wingless signalling activity. *Nature* **395**, 604–608 (1998).
61. M. van de Wetering, R. Cavallo, D. Dooijes, M. van Beest, J. van Es, J. Loureiro, A. Ypma, D. Hursh, T. Jones, A. Bejsovec, M. Peifer, M. Mortin, H. Clevers, Armadillo coactivates transcription driven by the product of the *Drosophila* segment polarity gene *dTCF*. *Cell* **88**, 789–799 (1997).
62. D. DaCrema, R. Bhandari, F. Karanja, R. Yano, A. Halme, Ecdysone regulates the *Drosophila* imaginal disc epithelial barrier, determining the length of regeneration checkpoint delay. *Development* **148**, dev195057 (2021).
63. R. E. Harris, M. J. Stinchfield, S. L. Nystrom, D. J. McKay, I. K. Hariharan, Damage-responsive, maturity-silenced enhancers regulate multiple genes that direct regeneration in *Drosophila*. *eLife* **9**, e58305 (2020).
64. E. Vizcaya-Molina, C. C. Klein, F. Serras, R. K. Mishra, R. Guigó, M. Corominas, Damage-responsive elements in *Drosophila* regeneration. *Genome Res.* **28**, 1852–1866 (2018).
65. K. J. Brennan, M. Weilert, S. Krueger, A. Pampari, H. Liu, A. W. H. Yang, J. A. Morrison, T. R. Hughes, C. A. Rushlow, A. Kundaje, J. Zeitlinger, Chromatin accessibility in the *Drosophila* embryo is determined by transcription factor pioneering and enhancer activation. *Dev. Cell* **58**, 1898–1916.e9 (2023).
66. C. Jiang, B. F. Pugh, Nucleosome positioning and gene regulation: Advances through genomics. *Nat. Rev. Genet.* **10**, 161–172 (2009).
67. J. D. Buenrostro, P. G. Giresi, L. C. Zaba, H. Y. Chang, W. J. Greenleaf, Transposition of native chromatin for fast and sensitive epigenomic profiling of open chromatin, DNA-binding proteins and nucleosome position. *Nat. Methods* **10**, 1213–1218 (2013).
68. S. E. Iismaa, X. Kaidonis, A. M. Nicks, N. Bogush, K. Kikuchi, N. Naqvi, R. P. Harvey, A. Husain, R. M. Graham, Comparative regenerative mechanisms across different mammalian tissues. *NPJ Regen Med* **3**, 6 (2018).
69. N. Suzuki, H. Ochi, Regeneration enhancers: A clue to reactivation of developmental genes. *Dev. Growth Differ.* **62**, 343–354 (2020).
70. M. Suzuki, A. Okumura, A. Chihara, Y. Shibata, T. Endo, M. Teramoto, K. Agata, M. E. Bronner, K. T. Suzuki, Fgf10 mutant newts regenerate normal hindlimbs despite severe developmental defects. *Proc. Natl. Acad. Sci. U.S.A.* **121**, e2314911121 (2024).
71. A. Kawasumi-Kita, S.-W. Lee, D. Ohtsuka, K. Niimi, Y. Asakura, K. Kitajima, Y. Sakane, K. Tamura, H. Ochi, K. T. Suzuki, Y. Morishita, *hoxc12/c13* as key regulators for rebooting the developmental program in *Xenopus* limb regeneration. *Nat. Commun.* **15**, 3340 (2024).
72. M. I. Worley, N. J. Everetts, R. Yasutomi, R. J. Chang, S. Saretha, N. Yosef, I. K. Hariharan, *Ets21C* sustains a pro-regenerative transcriptional program in blastema cells of *Drosophila* imaginal discs. *Curr. Biol.* **32**, 3350–3364.e6 (2022).
73. M. Iwafuchi-Doi, K. S. Zaret, Cell fate control by pioneer transcription factors. *Development* **143**, 1833–1837 (2016).
74. T. J. Gibson, E. D. Larson, M. M. Harrison, Protein-intrinsic properties and context-dependent effects regulate pioneer factor binding and function. *Nat. Struct. Mol. Biol.* **31**, 548–558 (2024).

75. M. Mir, M. R. Stadler, S. A. Ortiz, C. E. Hannon, M. M. Harrison, X. Darzacq, M. B. Eisen, Dynamic multifactor hubs interact transiently with sites of active transcription in *Drosophila* embryos. *eLife* **7**, e40497 (2018).
76. P. Heitzler, M. Bourouis, L. Ruel, C. Carteret, P. Simpson, Genes of the enhancer of split and achaete-scute complexes are required for a regulatory loop between Notch and Delta during lateral signalling in *Drosophila*. *Development* **122**, 161–171 (1996).
77. A. Baonza, A. Garcia-Bellido, Notch signaling directly controls cell proliferation in the *Drosophila* wing disc. *Proc. Natl. Acad. Sci. U.S.A.* **97**, 2609–2614 (2000).
78. C. Bergantiños, M. Corominas, F. Serras, Cell death-induced regeneration in wing imaginal discs requires JNK signalling. *Development* **137**, 1169–1179 (2010).
79. M. Bosch, J. Baguñà, F. Serras, Origin and proliferation of blastema cells during regeneration of *Drosophila* wing imaginal discs. *Int. J. Dev. Biol.* **52**, 1043–1050 (2008).
80. M. Bosch, F. Serras, E. Martín-Blanco, J. Baguñà, JNK signaling pathway required for wound healing in regenerating *Drosophila* wing imaginal discs. *Dev. Biol.* **280**, 73–86 (2005).
81. E. Blanco, M. Ruiz-Romero, S. Beltran, M. Bosch, A. Punset, F. Serras, M. Corominas, Gene expression following induction of regeneration in *Drosophila* wing imaginal discs. Expression profile of regenerating wing discs. *BMC Dev. Biol.* **10**, 94 (2010).
82. T. Katsuyama, F. Comoglio, M. Seimiya, E. Cabuy, R. Paro, During *Drosophila* disc regeneration, JAK/STAT coordinates cell proliferation with Dilp8-mediated developmental delay. *Proc. Natl. Acad. Sci. U.S.A.* **112**, E2327–E2336 (2015).
83. S. J. Khan, S. N. F. Abidi, A. Skinner, Y. Tian, R. K. Smith-Bolton, The *Drosophila* Duox maturation factor is a key component of a positive feedback loop that sustains regeneration signaling. *PLOS Genet.* **13**, e1006937 (2017).
84. X.-S. Zhang, L. Wei, W. Zhang, F.-X. Zhang, L. Li, L. Li, Y. Wen, J.-H. Zhang, S. Liu, D. Yuan, Y. Liu, C. Ren, S. Li, ERK-activated CK-2 triggers blastema formation during appendage regeneration. *Sci. Adv.* **10**, eadk8331 (2025).
85. A. R. Gehrke, E. Neverett, Y.-J. Luo, A. Brandt, L. Ricci, R. E. Hulett, A. Gompers, J. G. Ruby, D. S. Rokhsar, P. W. Reddien, M. Srivastava, Acoel genome reveals the regulatory landscape of whole-body regeneration. *Science* **363**, eaau6173 (2019).
86. M. C. Manansala, S. Min, M. D. Cleary, The *Drosophila* SERTAD protein Taranis determines lineage-specific neural progenitor proliferation patterns. *Dev. Biol.* **376**, 150–162 (2013).
87. M. M. Harrison, M. R. Botchan, T. W. Cline, Grainyhead and Zelda compete for binding to the promoters of the earliest-expressed *Drosophila* genes. *Dev. Biol.* **345**, 248–255 (2010).
88. B. Langmead, S. L. Salzberg, Fast gapped-read alignment with Bowtie 2. *Nat. Methods* **9**, 357–359 (2012).
89. H. Li, B. Handsaker, A. Wysoker, T. Fennell, J. Ruan, N. Homer, G. Marth, G. Abecasis, R. Durbin, 1000 Genome Project Data Processing Subgroup, The sequence alignment/map format and SAMtools. *Bioinformatics* **25**, 2078–2079 (2009).
90. P. Machanick, T. L. Bailey, MEME-ChIP: Motif analysis of large DNA datasets. *Bioinformatics* **27**, 1696–1697 (2011).
91. G. Cuellar-Partida, F. A. Buske, R. C. McLeay, T. Whitington, W. S. Noble, T. L. Bailey, Epigenetic priors for identifying active transcription factor binding sites. *Bioinformatics* **28**, 56–62 (2012).

Acknowledgments: We thank S. Mathure and F. Hsu for critical reading of the manuscript. We thank M. Harrison for providing many of the reagents used in this study. We would like to give a special thanks to BDSC (grant P40OD018537), DGRC, and DSHB for reagents. **Funding:** This work was supported by National Institute of Health, R01GM107140 (to R.K.S.-B.) and R35GM14174 (to R.K.S.-B.), and the Arnold O. Beckman Award from the University of Illinois, RB20123 (to R.K.S.-B.).
Author contributions: Conceptualization: A.B., K.S., S.S., and R.K.S.-B. Methodology: A.B., K.S., and S.S. Investigation: A.B., C.K., and K.S. Supervision: R.K.S.-B. Writing—original draft: A.B. and R.K.S.-B. Writing—review and editing: A.B., R.K.S.-B., K.S., S.S., and C.K. **Competing interests:** The authors declare that they have no competing interests. **Data and materials availability:** All data needed to evaluate the conclusions in the paper are present in the paper and/or the Supplementary Materials. Sequencing data for the CUT&RUN experiments are available from the GEO database, accession number GSE268674. All other relevant raw data are available at the Illinois Databank (https://doi.org/10.13012/B2IDB-6269288_V1).

Submitted 20 August 2024
Accepted 1 May 2025
Published 6 June 2025
10.1126/sciadv.ads5743